



## Review paper

## Printability—A key issue in extrusion-based bioprinting

Saman Naghieh <sup>a,\*</sup>, Xiongbiao Chen <sup>a,b,\*\*</sup><sup>a</sup> Division of Biomedical Engineering, College of Engineering, University of Saskatchewan, Saskatoon, SK, S7N 5A9, Canada<sup>b</sup> Department of Mechanical Engineering, College of Engineering, University of Saskatchewan, Saskatoon, SK, S7N 5A9, Canada

## ARTICLE INFO

## Article history:

Received 26 November 2019

Received in revised form

1 February 2021

Accepted 5 February 2021

Available online 10 February 2021

## Keywords:

Extrusion

3D bioprinting

Bioink

Printability

Tissue engineering

## ABSTRACT

Three-dimensional (3D) extrusion-based bioprinting is widely used in tissue engineering and regenerative medicine to create cell-incorporated constructs or scaffolds based on the extrusion technique. One critical issue in 3D extrusion-based bioprinting is printability or the capability to form and maintain reproducible 3D scaffolds from bioink (a mixture of biomaterials and cells). Research shows that printability can be affected by many factors or parameters, including those associated with the bioink, printing process, and scaffold design, but these are far from certain. This review highlights recent developments in the printability assessment of extrusion-based bioprinting with a focus on the definition of printability, printability measurements and characterization, and printability-affecting factors. Key issues and challenges related to printability are also identified and discussed, along with approaches or strategies for improving printability in extrusion-based bioprinting.

© 2021 Xi'an Jiaotong University. Production and hosting by Elsevier B.V. This is an open access article under the CC BY-NC-ND license (<http://creativecommons.org/licenses/by-nc-nd/4.0/>).

## 1. Introduction

The limited availability of appropriate organs to meet the increasing worldwide demand for transplantation has resulted in global organ shortage [1]. In the United States alone, more than 70,000 patients are waiting for organ transplants [2]. Tissue engineering (TE) has emerged as a promising method to regenerate human organs and tissues [3]. In particular, scaffold-based TE aims to develop bio-constructs, i.e., so-called scaffolds, to eventually replace, protect, restore, or repair damaged tissues, such as skin, bladder, trachea, and myocardium, after implantation [4–10]. Three-dimensional (3D) printing has been driving significant TE innovations, enabling the creation of variably complex biocompatible scaffolds suitable for transplantation [11]. One of the 3D printing techniques (also known as additive manufacturing (AM)) widely used in TE is extrusion- or dispensing-based bioprinting [11], where a mixture of biomaterials and cells (referred to as bioink) is dispensed or extruded, layer-by-layer, to form a 3D scaffold (Fig. 1) [12]. Typically, bioink needs to be crosslinked, a process that promotes solidification of its liquid form during or

after printing. Depending on their nature, bioinks can be physically or chemically cross-linked. Either way, scaffolds should be designed and printed so as to recapitulate the biological and mechanical properties of native tissue; these "biomimetic" scaffolds promote successful and functional tissue regeneration [13,14]. To this end, numerous efforts have been made to fabricate biomimetic scaffolds using extrusion-based bioprinting. This review focuses on the key issue of printability in the extrusion-based bioprinting process, highlighting the factors that can affect printability, reviewing methods to measure/characterize/improve printability, and identifying associated issues and challenges for future endeavors.

## 2. Definition of printability and its significance

Printability is the capability to form and maintain reproducible 3D scaffolds from bioink using the bioprinting technique. Printability affects the structure of the printed scaffolds, and as a result, affects their mechanical and biological properties. Live cell-incorporated structures can be fabricated using the extrusion-based bioprinting technique. For this purpose, hydrogels have been widely used because of their cell-friendly environment and high water content. Hydrogels can be crosslinked physically or chemically to facilitate the creation of a bioprinted 3D structure. The crosslinking of hydrogels is a time-intensive process, and as such, the hydrogel can flow or spread and thus substantially deviate from the desired design. Owing to the poor printability of hydrogels, printed scaffolds may sometimes even collapse and fail to

Peer review under responsibility of Xi'an Jiaotong University.

\* Corresponding author.

\*\* Corresponding author. Division of Biomedical Engineering, College of Engineering, University of Saskatchewan, Saskatoon, SK, S7N 5A9, Canada.

E-mail addresses: [san908@mail.usask.ca](mailto:san908@mail.usask.ca) (S. Naghieh), [xbc719@mail.usask.ca](mailto:xbc719@mail.usask.ca) (X. Chen).

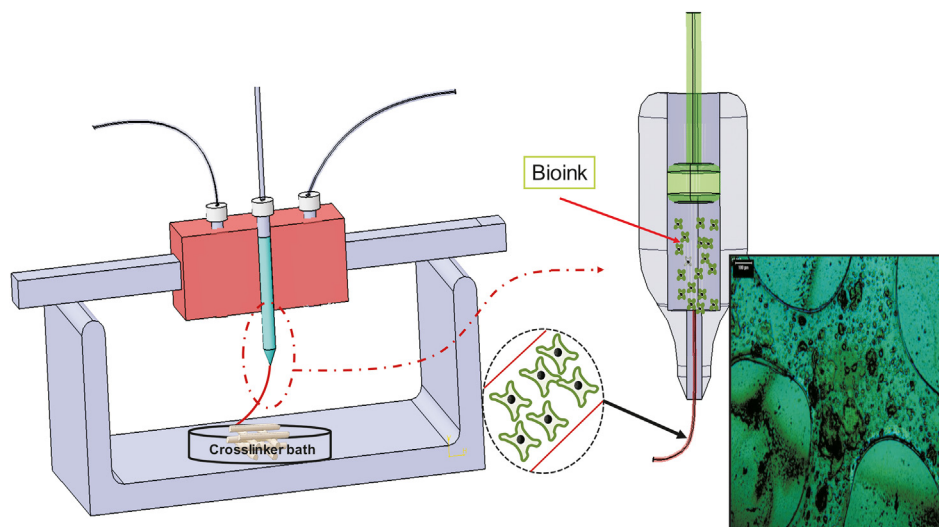


**Fig. 1.** Schematic of extrusion-based bioprinting technique (inset is a cell-incorporated alginate scaffold, reproduced with permission from Ref. [12]).

form a 3D structure. The printability concept is important because the difference between a printed scaffold and the ideal design can impact the mechanical and biological properties, including mechanical strength and cell functions [15–18].

Printability can affect the shape fidelity of bio-fabricated scaffolds generated using the extrusion-based technique, and by extension, cell performance [19–21]. Printability is essential in the sense that the structure of a scaffold controls the morphology and growth of cells after printing, the cultivation of which is already a challenging issue in TE [22]. Cell-incorporated hydrogels should be deposited as per designs intended to recapitulate the properties of natural organs or tissues because the printed structure can affect cell fate after printing [22]. Poor printability can cause cell damage and result in tissue malfunction. Cell printing studies are also often quite expensive, so determining the correct printing parameters by trial and error is impractical [23]. Finally, yet importantly, printability affects the mechanical behavior of the 3D-printed scaffolds.

### 3. Key factors affecting printability

The factors affecting printability can be classified into three categories: scaffold design, bioink, and printing process (Fig. 2) [24]. These will be elaborated upon in detail in subsequent sections. Briefly, scaffold design-related parameters that can influence printability include the pore size (spacing) strand (filament) orientation, and layer thickness. Two critical factors related to the bioink are its flow behavior and physical properties. Relevant printing process parameters include the crosslinking mechanism and printing parameters such as pressure and speed.

#### 3.1. Scaffold design and printability

Several factors associated with scaffold design influence printability, including strand orientation, pore size (spacing), and layer thickness. However, a limited number of studies have identified key elements that play a significant role in printability from a scaffold design perspective.

The orientation of strands dictates the configuration and inner pattern of a designed model based on layer-upon-layer printing to create a 3D scaffold (Fig. 3). Strand orientation can affect the surface porosity of a scaffold (side-walls), by 5- to 10-fold, and also the overall porosity [25]. Furthermore, the orientation of the strands

can affect the amount of deposited bioink. Changing each strand's orientation near the edge of the scaffold to 45° instead of 90° requires a smaller amount of bioink; larger pore sizes can also be achieved using a 45° inner pattern [25]. Since 2000, many studies have emphasized the effect of strand orientation on the mechanical properties of scaffolds [26–28].

Several studies have considered the effect of pore size on cell performance [15,16] and mechanical properties [17,18]. More specifically, numerous studies have considered the impact of strand orientation on mechanical properties, but few have considered the effect on printability. One study showed that the distance between strands, defined as the pore size, of a scaffold selected in a model can affect the printability of scaffolds made of a mixture of carboxymethylcellulose and alginate [29]. A filament collapse test can be used to investigate the effect of pore size on printing quality [29–31]. However, little is known about the effect of pore size on the printability and structural integrity of printed hydrogels.

Layer thickness is another scaffold-design-related parameter. Some studies consider the effect of layer thickness on the geometric accuracy and printing process time [15]. Layer thickness can influence pore size, and changing the layer thickness during printing can achieve more accurate pore sizes [32]. The main reason for changing the layer thickness during the printing process is that, from the top to the bottom of a scaffold, the pore size does not remain constant when a constant layer thickness is used during the printing process. This change in pore size is due to the weight of subsequent layers and pressure fluctuation during the printing process. Scaffolds with more accurate geometries have been fabricated using smaller layer thicknesses. A recent study showed that a 30 μm increase in layer thickness not only improved the production rate but also had no effect on the fatigue performance, dimensions, and geometry of scaffolds [33]. Nonetheless, few studies have considered the effects of layer thickness on printability [15]. Fig. 4 [15] shows the effect of layer thickness on the accuracy of a printed scaffold. More systematic studies are needed to investigate the effect of layer thickness on the printability of printed scaffolds.

In recent years, extrusion-based bioprinting has enabled the possibility of printing advanced constructs such as those with gradient constructions. For instance, some studies have aimed to replicate the zonal structure of cartilage by improving the scaffold design [34]. Other studies have focused on the creation of human-

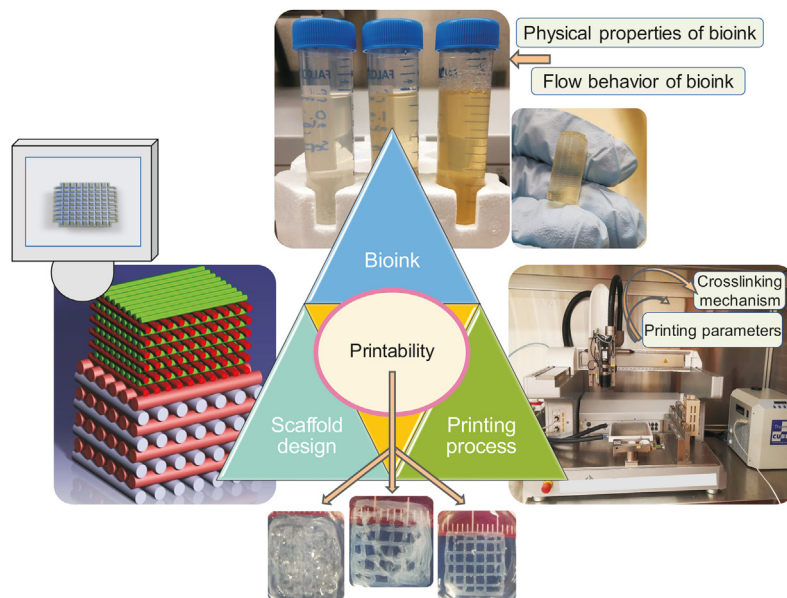


**Fig. 2.** Key factors affecting the printability of scaffolds fabricated by the extrusion-based 3D bioprinting technique (reproduced with permission from Ref. [24]).

scale tissue structures with structural integrity [1]. Based on the application, different patterns can be used to create such complex structures. 3D hydrogel square honeycomb scaffolds have been created using the AM technique, as this pattern can facilitate *in vitro* studies on hippocampal neurons; honeycomb patterns have also been used to induce spheroid formation by human bone mesenchymal cells to enhance differentiation [35]. Zigzag is another type of pattern used to create hydrogel scaffolds that need any type of support owing to its curvature and has been implemented to create complex tissue structures [36]. Square waveform patterns are also used for hydrogel scaffold creation. This pattern enhances nutrient and drug diffusion to the core of the strands extruded layer-by-layer, and its high surface area to volume ratio makes it useful for introducing structural cues [37]. Space-filling is another type of pattern used for continuous extrusion to improve the printability of complex constructs [38]. This pattern has also been used to facilitate cell adhesion and faster growth [39]. Despite this progress, there is much potential for further development [15], i.e., production of constructs with clinically relevant sizes and structural integrity. With respect to constructs with clinically

relevant dimensions, the major challenge is the feasibility of studies focusing on the printability of these constructs. To this end, the use of supports is a common approach; supports are required in the printing of almost all complex constructs (such as ears) [11]. Another gap in research is related to the printability of functionally graded structures, such as zonal scaffolds. Functionally graded structures involve gradationally changing the material organization within a structure to accomplish an intended function; however, little is known about the bioprinting of such structures [40,41]. A process for printing functionally graded scaffolds and determining their printability through extrusion-based bioprinting is yet to be developed. Quite often, simple cubic scaffolds are fabricated.

Several patterns, such as zigzag and honeycomb, have been used to inspire other researchers to develop novel structures with interconnected pores for scaffold fabrication (investigating the influence of strand arrangement/pattern, Fig. 5). Furthermore, scaffolds can be designed to be printed on either the inside or outside of a defined border. Thereafter, continuous and non-continuous strands can be selected during the scaffold design procedure, which also might affect printability (Fig. 5).

A deflection test can be conducted to study the effect of pore size on printability (Fig. 6). Some studies have conducted filament collapse tests to determine the effect of pore size on printability and shown the significance of pore size on printing quality [29–31]. However, little is known about the effect of pore size on the printability and structural integrity of printed hydrogels. As noted above, most studies focus on the influence of pore size on either the behavior of cell or the mechanical properties of the scaffold. The deflection test tool can evaluate different pore sizes in terms of deflection. To this end, the effect of pore size (selected during scaffold design) on printability is investigated by comparing the actual and theoretical areas.

From a layer thickness perspective, scaffolds can be fabricated according to different designs that assign different thicknesses to other layers. The geometric accuracy and printing process time can be affected by modulating the layer thickness [15]; however, more accurate pore sizes can be achieved by changing the layer thickness during the printing process [32]. For example, an increase in the layer thickness of only 30  $\mu\text{m}$  can improve the production rate and printability [15,33]. Fig. 7 shows a 7 mm  $\times$  7 mm  $\times$  5 mm cubic

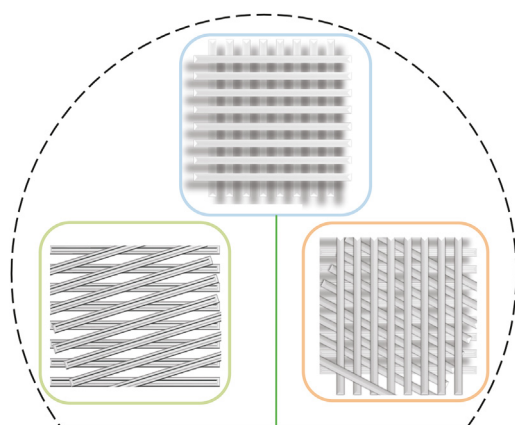


**Fig. 3.** Schematic of scaffolds with different strand orientations ( $0^\circ$ ,  $45^\circ$ ,  $60^\circ$ ,  $90^\circ$ – $120^\circ$ , and  $135^\circ$ ).

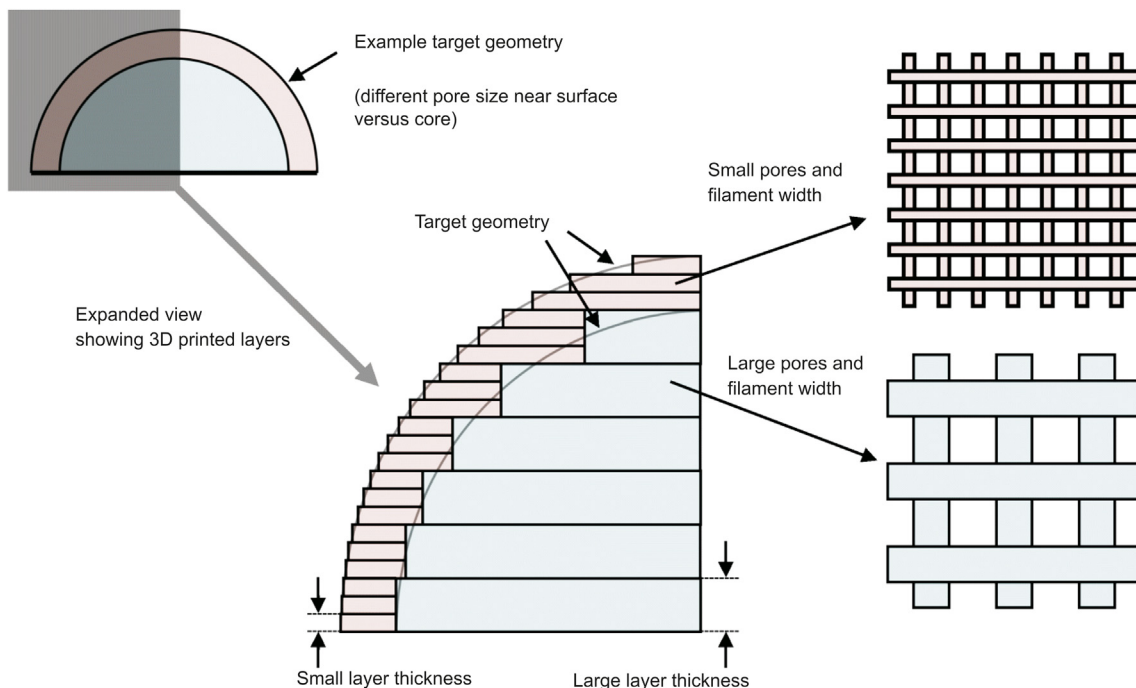


Fig. 4. Effect of layer thickness on scaffolds' printability and dimensions (reproduced with permission from Ref. [15]).

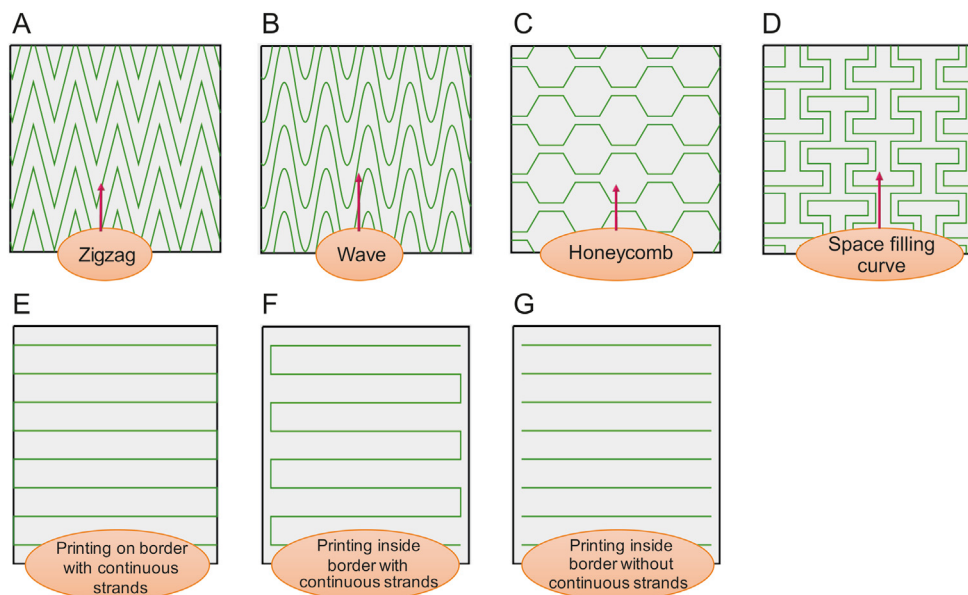


Fig. 5. Different patterns for scaffold printing: (A) zigzag, (B) wave, (C) honeycomb, (D) space-filling curve, (E) printing, (F) on border with continuous strands, and (G) inside border with continuous strands and inside border without continuous strands.

model for which the software automatically calculates the number of layers after assigning the layer thickness (16, 24, 30, 49, and 99 layers for thicknesses of 300, 200, 160, 100, and 50  $\mu\text{m}$ , respectively). This illustration shows the importance of layer thickness because, even before printing, the calculated thickness of the cubic model varies between 4.8 and 4.95 mm (the original height of the designed model is 5 mm) based on the number of layers. The inclusion properties of the designed model during the slicing process and assigning the layer thickness can also influence printability. Several inclusion options, such as no inclusion, inlying, centric, and outlying, are available for selection during the scaffold design procedure.

Scaffolds can be fabricated with or without support, as shown in Fig. 8 (the contour acts as a support). Supports can play a critical role in the resolution of printing and accuracy [11,42], so it is vital to consider printability effects. In some cases, printing is impossible without any support [43].

### 3.2. Bioink and printability

Another factor affecting printability is the composition of the bioink used for scaffold fabrication. This factor includes the flow behavior and physical properties. Some studies have considered the flow behavior of bioinks to evaluate printability [44,45], although

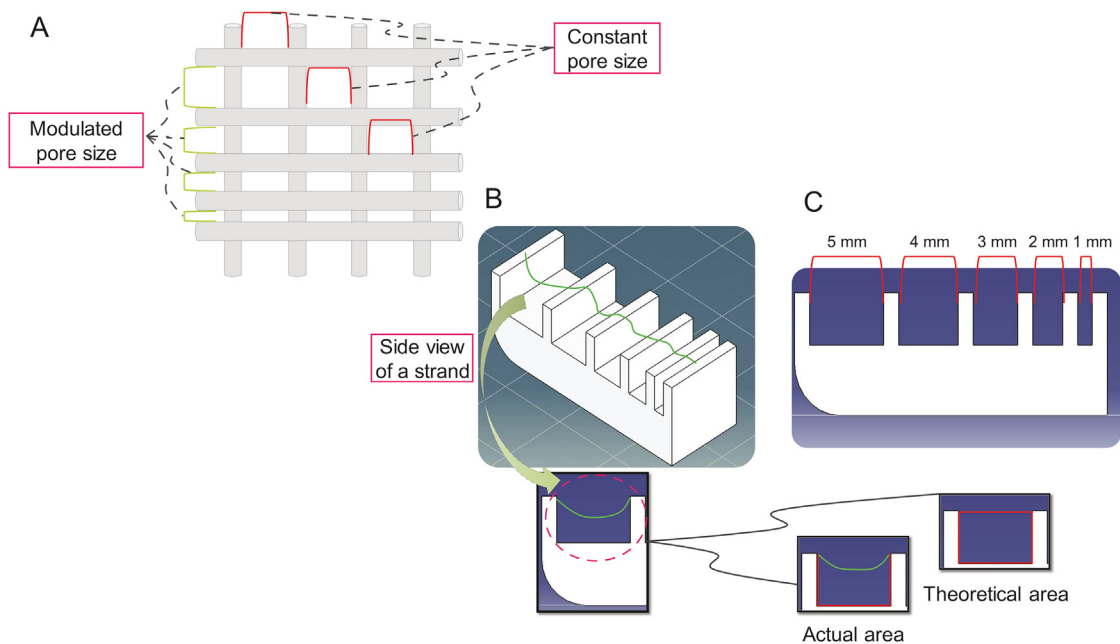


**Fig. 6.** Filament collapse test to measure the effect of deflection of scaffold strands: (A) modulated pore size while keeping the pore size constant in the opposite direction, (B) deflection test benchmark (actual and theoretical areas), and (C) side view of a deflection test benchmark.

they have only investigated the rheological characteristics [46]. However, the physical properties of bioinks, such as the contact angle, surface tension, and roughness, should also be studied to determine their effect on printability.

The flow behavior of bioinks used for scaffold biofabrication has been thoroughly investigated in different studies [45,47,48]. A recent study focused on the effect of loss and storage modulus on scaffold printability [47]. However, the physical properties of bioinks, such as the contact angle and surface tension, have been neglected. These characteristics might also affect cell performance, such as cell seeding and cell proliferation [15,17,18,49].

Several types of hydrocarbon bioinks can be used for scaffold fabrication. Polysaccharide-based hydrogels are frequently used

because of their positive effects on cell migration, axonal guidance, and synaptic development [50,51]. One polysaccharide-based hydrogel that is widely used in extrusion-based bioprinting is alginate, owing to its biocompatibility, low toxicity, and relatively high printability [52–54]. Alginate is an excellent substrate to incorporate pancreatic islet cells, fibroblasts, myoblasts, and chondrocytes [55]. As this review does not aim to cover all hydrogel bioinks used in extrusion-based bioprinting, only a few are introduced in this section, and some examples related to alginate are discussed. Interested readers are directed to a recent review of soft bioinks used in extrusion-based bioprinting [56].

Other types of bioinks are sometimes mixed with alginate to create hybrid or composite scaffolds. The objective is to improve

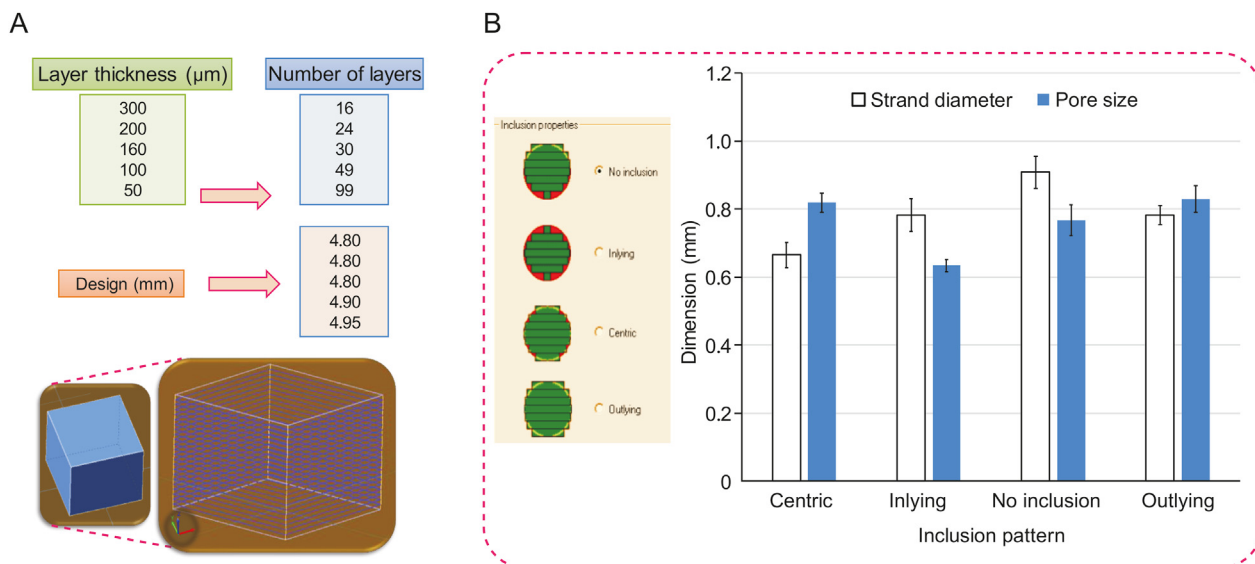


**Fig. 7.** (A) Effect of layer thickness selected during scaffold design on the printability of bioplotted scaffolds. (B) The impact of the inclusion pattern chosen on pore size and strand diameter of bioplotted alginate scaffolds (constant printing parameters and conditions).

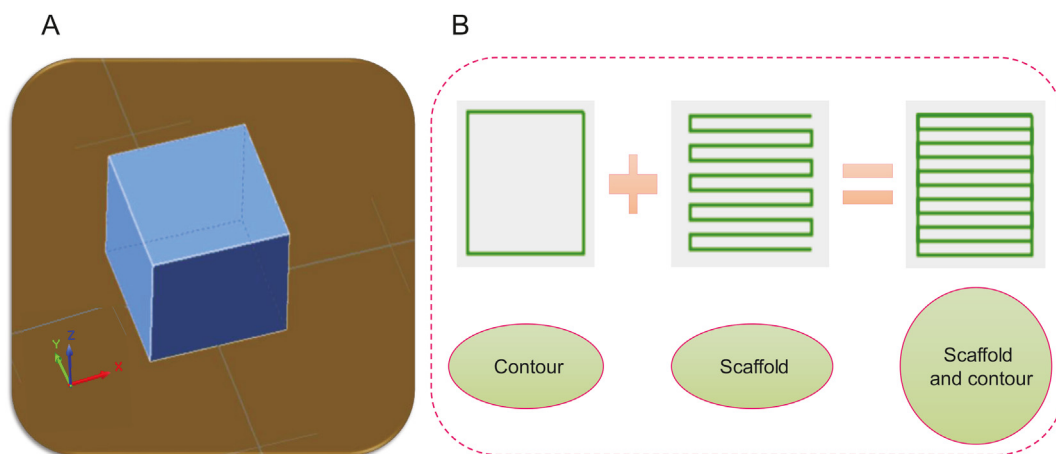


Fig. 8. Scaffold design: (A) a regular cubic design, and (B) the creation of patterns with or without contours/support.

the printability, mechanical properties, and biological characteristics of alginate scaffolds [57]. For instance, alginate does not have the adhesion sites required for cell attachment; scaffolds made of alginate and gelatin can be an excellent solution to address this issue and improve the biological properties of alginate scaffolds [58]. Gelatin is also widely used to improve the mechanical properties and printability of hydrogel scaffolds; for instance, adding gelatin to alginate can improve printability [45]. Gelatin is a collagen derivative that is less expensive than pure collagen and lacks collagen's antigenicity, thus reducing the possibility of an immunological response from the host in which the scaffold is implanted [59]. Pan et al. [60] analyzed the properties of scaffolds containing both gelatin and alginate and found high water retention rates. In another study, marine eel fish skin collagen was mixed with alginate to improve printability [61]. These studies suggest that combining different bioinks may help manipulate scaffold characteristics and allow for better control to achieve the desired scaffold functions. To this end, using a mixture of bioinks can also improve printability. Gelatin and alginate behave like elastic and viscous bioinks, respectively. Their combination shows synergetic effects; for example, the loss and storage moduli can be modulated by adjusting the alginate and gelatin concentrations in the mixture [47]. Importantly, creating hybrid or non-hybrid scaffolds requires materials that are printable, but not all bioinks meet this requirement.

At the liquid-air interface, surface tension occurs because the attraction of liquid molecules is more significant than that of molecules in the air (Newton/length or energy/m<sup>2</sup>). Many studies have neglected the effect of surface tension on printability. This aspect is typically studied in inkjet-based printers [62–64]; however, it can clearly affect the printability of scaffolds fabricated by extrusion-based bioprinting techniques. Surface tension is the liquid-vapor interfacial energy and can affect printability in terms of the contact angle between the two media. It can also influence the printing quality, resolution, and strand diameter [65,66]. The contact angle is a measure used to evaluate the hydrophilicity of a scaffold; a hydrophilic scaffold can potentially improve cell growth as it has good wettability, which improves biological behavior [67].

As a general rule, if the printing substrate has a high surface energy compared to the bioink's surface tension, the bioink will spread. Conversely, a low-energy substrate will result in less spread and a higher contact angle [68,69]. Moreover, a filament extruded from a nozzle is a building block for an extrusion-based fabricated scaffold. Hence, it is important to understand filament formation and the influencing factors. Generally, surface tension and gravity

are critical factors affecting filament formation and printability [70].

Most bioinks used in extrusion-based bioprinting have shear thinning effects. That said, a high nozzle speed can lead to lower viscosities and, as a result, a larger surface tension. Generally, filaments deposited at high flow rates have lower viscosity and show smooth surfaces (larger surface tension) when exiting the nozzle [43]. To manipulate the surface tension and surface energy of the substrate, different approaches can be implemented to improve printability or limit excessive bioink spreading. First, the printing substrate can be treated with a hydrophobic material to provide a low-energy surface. This means that even bioinks with low surface tension will not spread. Substrate surface treatment has been introduced as an appropriate technique to modulate the substrate's surface energy [71]. Second, a highly viscous bioink can be used to minimize the spread [69]. However, not all high-viscosity bioinks are recommended because of the need for high pressure to facilitate extrusion and the consequent disruptive effects on cell viability [72]. Third, a faster crosslinking or drying rate is another solution to improving printing resolution and, consequently, printability [69,73]. This can be achieved by modulating the scaffold's crosslinking mechanism or porosity (the higher the porosity, the faster the rate of crosslinking). Another factor to be taken into account in a printability study is the type of needle used for printing. With respect to the interaction between the bioink and needle, the needle surface energy must also be considered.

Different tests can be performed to investigate the surface tension. Because materials are in direct contact with the substrate to print the first layer, the substrate's surface and surface energy are essential. Fig. 9 [74] shows the contact angle for non-coated glass, polyethylenimine-coated glass, and gelatin-coated glass slides, showing that glass slides coated with gelatin and polyethylenimine result in a smaller contact angle. This might be due to the hydrophilic nature of gelatin. Polyethylenimine is widely used as a glue that provides a sticky substrate to print the first layer of scaffolds in a crosslinker [73,75]. Thus, a trade-off occurs: a 180 contact angle is not always the best scenario because of difficulties related to attaching the first layer to the substrate, but a bioink with high wettability spreads the material over the substrate, moving far away from the ideal design.

A small contact angle can be interpreted as a surface with high wettability or a bioink with low surface tension. However, this is not the ideal case when it comes to printability. To achieve appropriate printability, scaffolds should be fabricated as per the scaffold design with the bioink not spreading during the printing

process (contact angle=180°), but this may not happen due to gravity and the flow behavior of the bioink (e.g., viscosity). As Fig. 10 shows, 3D printed scaffolds may have a fluctuating strand diameter (Fig. 10B), penetration amongst layers (Fig. 10E), and deflection (Fig. 10D) [12].

Beyond considering the substrate, the contact angle of the bioink should be considered because after the first layer, the material is printed on other layers of the same bioink. The contact angle and, subsequently, the surface tension can be measured by investigating the cross-sectional profile of the extruded filaments. The following Eq. (1) can be used to estimate the contact angle and surface tension [76].

$$Q = \frac{1}{4} \pi D_N^2 v_{ink} = \frac{1}{4} \pi D_E^2 v_{path} \quad (1)$$

where  $Q$  is the flow rate,  $D_E$  is the diameter of the extruded filament,  $D_N$  is the needle diameter,  $v_{ink}$  is the speed of the extruded filament, and  $v_{path}$  is the nozzle speed (Fig. 11) [76]. If a constant volume is considered for an extruded bioink, then  $D_E$  can be calculated using Eq. (2).

$$D_E = \sqrt{\frac{v_{ink} D_N}{v_{path}}} \quad (2)$$

Fig. 11 [76] shows that printing a cylindrical filament is impossible because of surface tension and gravity; therefore, a cambered cross-section can be considered. This cambered cross-sectional area can be represented by Eq. (3). Using Eq. (3),  $R$  (the radius of the cambered profile) can be obtained, as shown in Eq. (4) ( $\theta$  is the contact angle).

$$\frac{1}{4} \pi D_E^2 = \frac{2\theta}{360^\circ} \pi R^2 - R^2 \sin \theta \cos \theta \quad (3)$$

$$R = \sqrt{\frac{\pi}{4\theta - 2 \sin 2\theta}} D_E \quad (4)$$

$R$  can also be obtained from Eq. (5) and by considering Eqs. (4) and (5), the height ( $H$ ) can be estimated as per Eq. (6).

$$R = \frac{1}{1 - \cos \theta} \quad (5)$$

$$H = \frac{(1 - \cos \theta) \sqrt{\pi} D_E}{\sqrt{4\theta - 2 \sin 2\theta}} \quad (6)$$

Using Eq. (6),  $H$  can be estimated and, finally, the surface tension ( $\gamma$ ) can be estimated using Eq. (7):

$$H = \sqrt{\frac{2\gamma(1 - \cos \theta)}{g \rho}}, \quad (7)$$

where  $g$  equals 9.8 m/s<sup>2</sup> and  $\rho$  is the density.

Surface wettability is usually measured by determining the droplet contact angle. However, the droplet profile depends on other factors such as gravity, adsorption, and the physical properties of the solid, gas, and liquid. A size-dependent contact angle cannot represent the surface tension and surface wettability, so it is crucial to determine an asymptotic contact angle ( $\theta_s$ ). Eq. (8) can be used as follows [77]:

$$R = \left[ \frac{3 \times \text{droplet volume}}{\pi (2 + \cos \theta_s) (1 - \cos \theta_s)^2} \right]^{1/3} \sin^2 \theta_s \quad (8)$$

where  $R$  is the filament radius, as shown in Fig. 11 [76].

In addition, the surface energy of the nozzle can cause excessive spreading of the bioink, so needle types should be investigated. The surface tension resistance at the nozzle tip and the material wettability in terms of the degree of affinity between a liquid and the nozzle surface can affect printability. In this regard, needles with different shapes (e.g., cylindrical or tapered) and materials (such as metal, plastic, and metal-plastic) can be used. Furthermore, surface roughness is often targeted to modify the surface wettability. Surface imperfections such as roughness can cause contact angle hysteresis. Surface wettability, contact angle, and surface tension are related, so it is vital to study surface roughness [77]. Surface roughness can be compared to the contact angle to identify a relationship. Fig. 12 shows the surface fluctuation of a

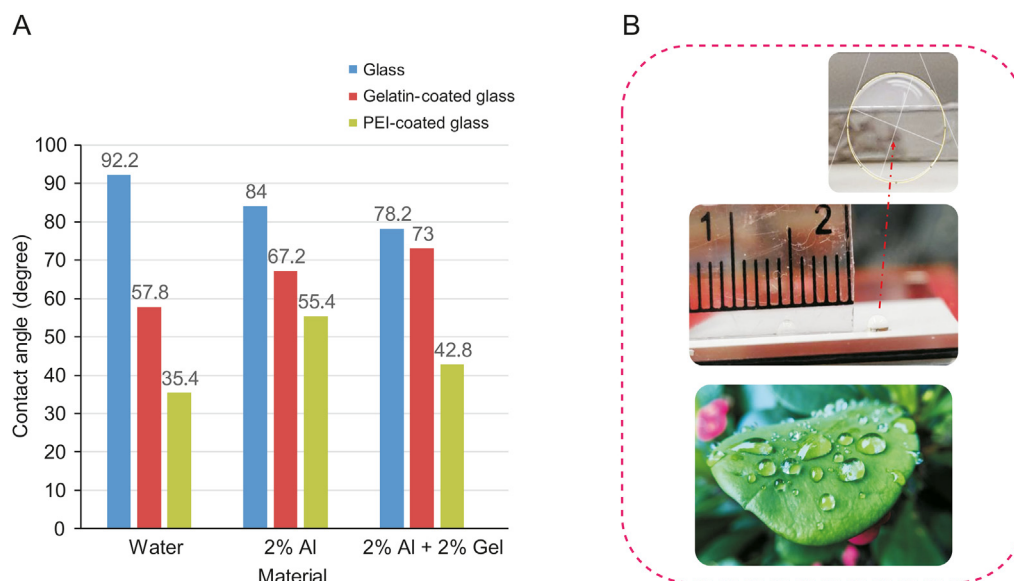
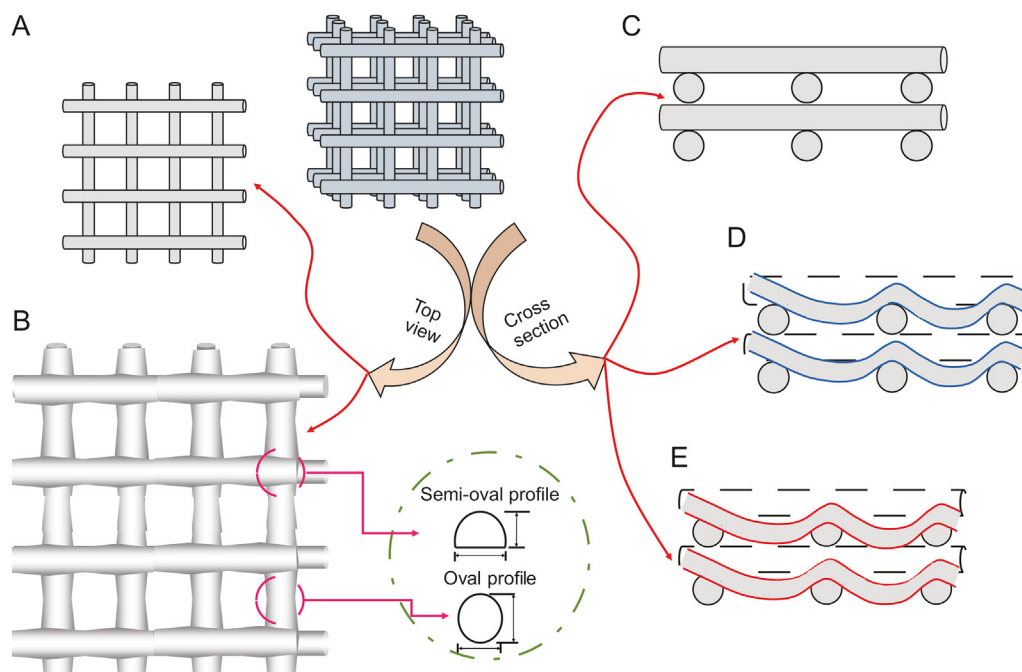


Fig. 9. Effect of the substrate (glass) surface energy on the contact angle of (A) different materials including water, 2% alginate (Al) and 2% Al + 2% gelatin (Gel) and (B) glass slide (inset shows contact angle) and image showing droplets of water on a leaf [74]. PEI: polyethylenimine.



**Fig. 10.** Idealistic and realistic views of printed scaffolds: top views with (A) idealistically constant and (B) fluctuating strand diameter; and side views with (C) no overlap among layers and no deflection, (D) no overlap and deflection, and (E) overlap and deflection (reproduced with permission from Ref. [12]).

printed scaffold and the surface roughness of the substrate. For example, a glass slide has a smooth surface with a roughness ( $R_a$ ) of  $0.01 \mu\text{m}$ , and a coated glass slide can have an  $R_a$  of  $1.02 \mu\text{m}$ ; the rougher surface can prevent the bioink from spreading. In other words, strands printed on a coated glass slide have higher contact angles and less spreading than those printed on a smooth glass slide.

Fig. 13 shows some results related to printability in terms of surface tension and contact angle for three groups of bioinks: 2% alginate, 2% alginate + 2% gelatin, and 2% alginate + 4% gelatin. The nozzle speed can affect both pore size and strand diameter, increasing the speed, decreasing the strand diameter, and

increasing the pore size (with other printing parameters held constant). The cross-sectional area also decreases with increasing nozzle speed. However, nozzle speed does not significantly affect the contact angle until the point that increasing the speed decreases the contact angle. Using Eq. (7), the relationship between surface tension and speed is mapped, showing that higher speeds lead to lower surface tension. The crosslinking mechanism plays a decisive role here as it solidifies the hydrogel (a droplet of a crosslinked hydrogel may have a different contact angle from a non-crosslinked one). That being said, the nozzle speed should be selected with respect to contact angle and surface tension. However, this is not an easy choice, as many interconnected elements affect printability. Apart from the effect on printability, surface interactions significantly affect the ink-cell interface and cellular functions. Drawing general conclusions is challenging: on the one hand, higher contact angles may result in relatively better printability; on the other hand, contact angles between  $60^\circ$  and  $70^\circ$  have the best surface energy and support appropriate cell functions [78].

### 3.3. Printing process and printability

Printing parameters and conditions affect printability, which is especially significant for printing complex 3D constructs with heterogeneous configurations. Printing conditions such as needle diameter, pressure, and printing speed can influence printability in terms of printing resolution, so studying such process-related elements is essential for a better understanding of them [76]. Numerous studies on printability have investigated the effect of printing parameters, such as air pressure and nozzle speed, which play the most decisive role in the printability of scaffolds fabricated by bioplotting, an extrusion-based technique [22,65,79].

From a printing process perspective, the crosslinking mechanism of scaffolds is also crucial as it affects the printability of bioink; however, little is known about this effect. In an extrusion-based system, cell-incorporated hydrogels are extruded layer-upon-layer. Extruded hydrogels, such as alginate precursors, need to be

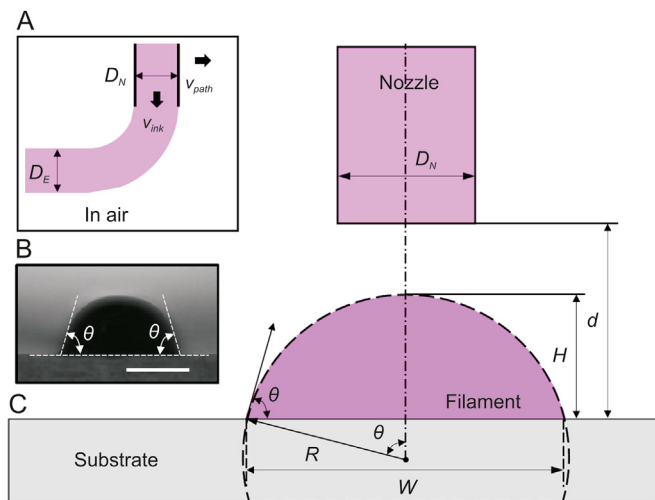


**Fig. 11.** Filament extrusion schematic: (A) needle diameter ( $D_N$ ), filament diameter ( $D_E$ ), nozzle speed ( $v_{path}$ ), and bioink speed ( $v_{ink}$ ), (B) contact angle of an extruded filament ( $\theta$ ), and (C) offset:  $d$ : distance between needle and substrate;  $H$ : filament height;  $W$ : filament width; and  $R$ : filament radius (reproduced with permission from Ref. [76]).

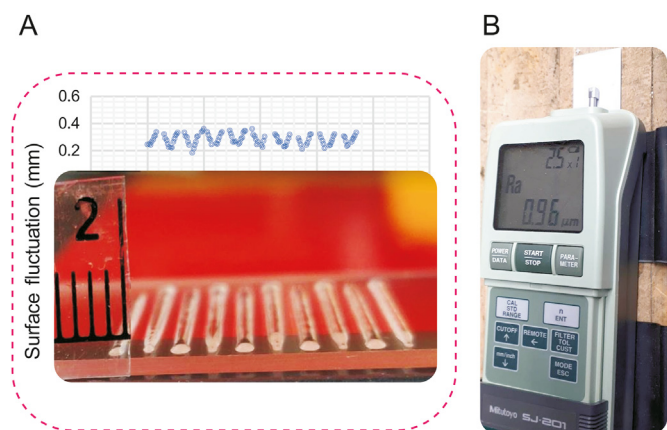


**Fig. 12.** Bioplotting strands on a glass slide: (A) the graph shows the surface fluctuation, and (B) the machine displays the roughness (Ra) of a coated glass slide.

gelled quickly to support the printing process and increase cell survival [80,81]. Divalent ionic crosslinkers, especially calcium chloride (CaCl<sub>2</sub>), have been widely implemented to crosslink hydrogels. One vital factor that should be considered is the

crosslinking and stability of hydrogels after fabrication. Although crosslinking is an excellent method to improve hydrogel printability, it is not reproducible [82]. Several studies also report that excessive crosslinking causes a significant reduction in cell viability in biofabrication [83]. In addition, the type and concentration of crosslinkers regulate the printing parameters (e.g., dispensing pressure and needle speed) and mechanical properties of 3D scaffolds. The hydrogel network density, which can be affected by the crosslinker type/concentration, is correlated with stiffness. Based on published reports, the higher the stiffness, the more significant the reduction in permeability of the hydrogel (less cell viability and proliferation of neural stem cells encapsulated in a hydrogel) [84]. Therefore, low-concentration crosslinkers are recommended. However, the critical challenge to be addressed is the poor printability of hydrogels crosslinked by a low crosslinker concentration. In this regard, the effects of crosslinking time and the amount of crosslinking agent solution have been neglected in the literature, as only the crosslinker concentration has been investigated. An appropriate amount of crosslinker solution should be used to minimize the depletion effect; however, this has not been well studied, and the proper crosslinker volume for an extrusion-based system remains to be determined [73]. Fig. 14 [73] shows a recent study on the effect of crosslinking time and volume on the elastic

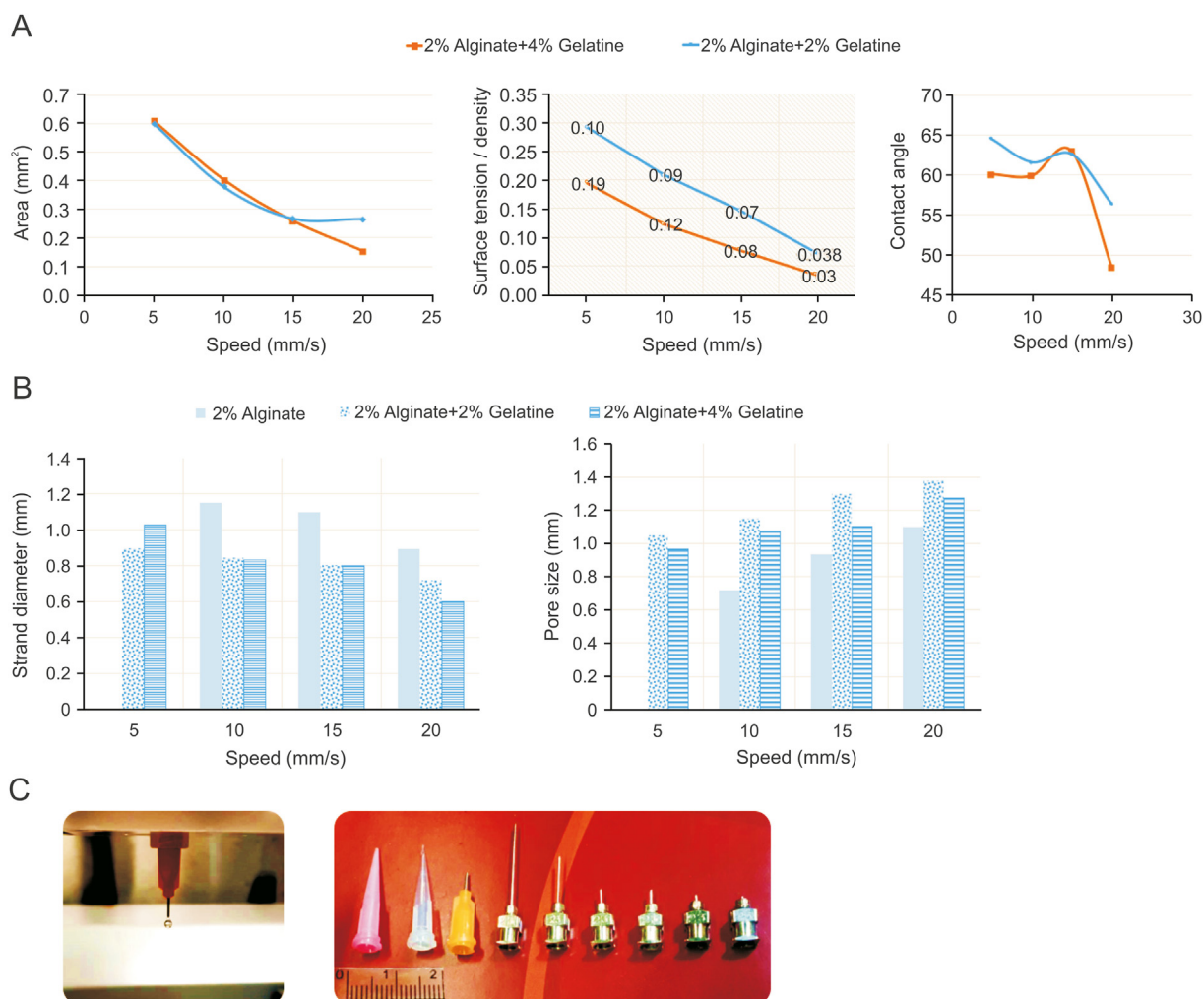


**Fig. 13.** Surface tension and contact angle studies for alginate-gelatin composite scaffolds: the effect of speed on (A) area, surface tension, and contact angle, (B) pore size and strand diameter (morphological studies), and (C) various types of needles.

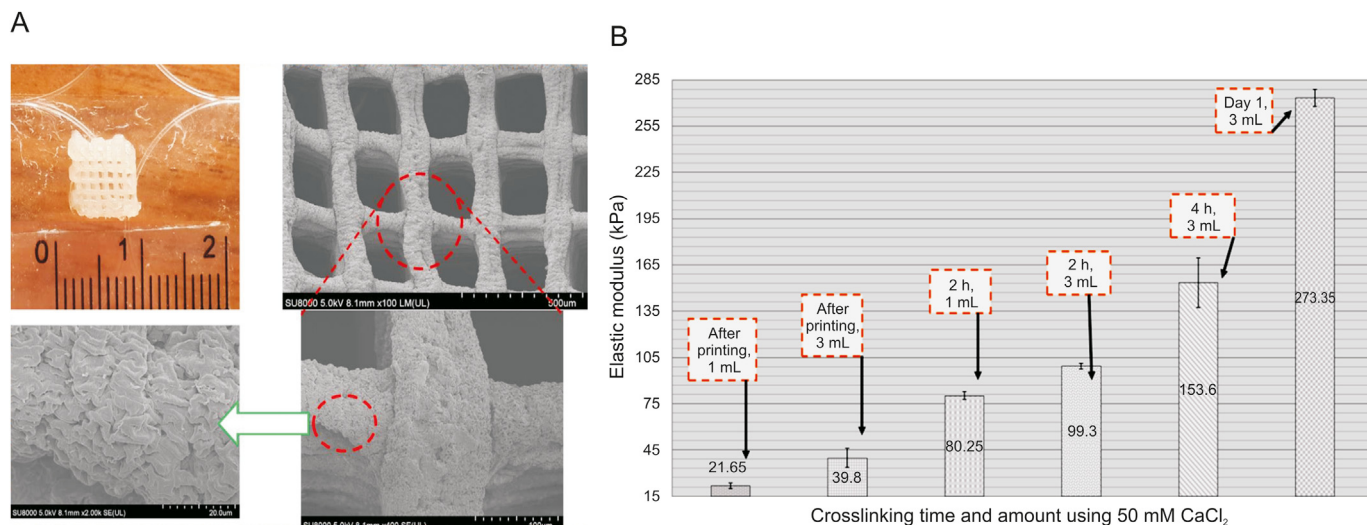


**Fig. 14.** (A) A bioplotting alginate scaffold (top left) and scanning electron microscopy (SEM) images after immersion in 50 mM CaCl<sub>2</sub> for 24 h. (B) The effect of crosslinking time and crosslinker volume on the elastic modulus of alginate scaffolds immersed in 1 mL or 3 mL of CaCl<sub>2</sub> (reproduced with permission from Ref. [73]).

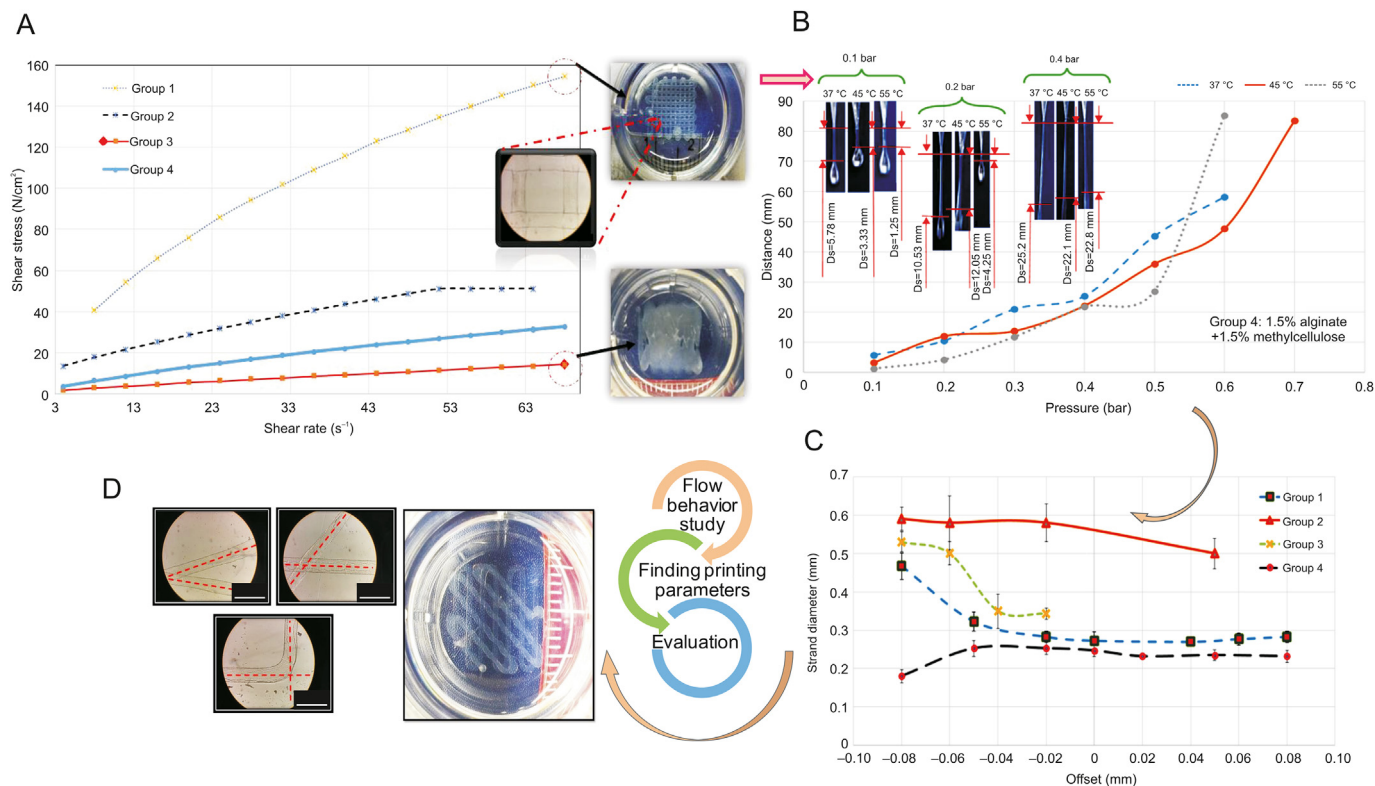


**Fig. 15.** Illustration of a common procedure to evaluate printability: (A) flow behaviour study to find the appropriate (B) pressure, (C) offset, and (D) angular pattern; group 1 (3% alginate), group 2 (2% alginate + 1% gelatin), group 3 (1.5% alginate + 1% gelatin + 0.5% methylcellulose), and group 4 (1.5% alginate + 1.5% methylcellulose) (reproduced with permission from Ref. [24]).

modulus of 3D bioplotting alginate scaffolds. Overall, the cross-linking mechanism can affect printability as different crosslinkers at various concentrations can affect the scaffold morphology [85]. Other techniques, such as coaxial nozzle printing, can be implemented to control the crosslinking mechanism properly. Readers are encouraged to refer to recent reports on coaxial nozzle printing [11,86–88].

While the goal of most studies is to construct an overall map of the relationships between hydrogel printability and various

printing parameters, they fail because of the presence of too many independent and inter-correlated factors that affect printability (e.g., pressure, nozzle speed and offset, and crosslinking mechanism). A consequence is the difficulty in explaining the results. As indicated in Fig. 2 [24], the printing process, scaffold design, and bioink are inter-related factors affecting printability, so determining the effect of each factor on printability is difficult. As such, printability studies often start by evaluating the flow behavior of the bioink to ensure that it has sufficient viscosity and is printable

**Table 1**  
Key factors influencing the printability of extrusion-based printed scaffolds.

Elements affecting printability	Bioinks	Results	Refs.
<b>Bioink-related factors</b>			
<i>Flow behavior and bioink composition</i>			
	Chitosan, chitosan-collagen, and methylcellulose-hyaluronan	Higher printability of bioinks with higher viscosity.	[91]
	Oxidized alginate	Viscosity in the range of 400–3000 mm <sup>2</sup> /s has a relatively high printability.	[92]
	Methacrylated hyaluronic acid and methacrylated gelatin	Highly viscous bioinks are not printable; similarly, low viscosity bioinks have poor printability.	[93]
	Alginate-nanocellulose	Nanocellulose can improve the printability of alginate by increasing viscosity.	[94]
	Collagen, gelatin, methacryloyl	Adding collagen can improve printability in terms of fidelity.	[95]
	Alginate-graphene oxide	Adding graphene oxide to alginate to modulate the flow behavior can improve printability.	[96]
	Alginate-gelatin	Addition of gelatin to alginate results in a significant improvement in printability.	[45,97]
	Lithium oxide-based inks	There is a trade-off: on the one hand, printing a highly viscous bioink is challenging due to high-pressure requirements; on the other hand, low viscosity bioinks are plagued with surface wetting problems.	[98]
<i>Physical properties</i>			
Surface tension, surface energy, and contact angle	Various materials	Substrates with lower surface energy result in reduced bioink spreading during the printing process. A contact angle of 90° was also reported as optimum; a lower contact angle means more spreading. Additionally, the nozzle type should be carefully selected as nozzles' surface energy can affect printability (high surface energy needles result in a high degree of capillary rise).	[99]
	Polydimethylsiloxane	Printing a relatively small construct can result in poor printability due to the significant effect of surface tension and its subsequent flow resistance.	[69]
<b>Scaffold design-related factors</b>			
<i>Pore size</i>			
<i>Dimension and grid geometry</i>			
<i>Angle and orientation</i>			
	Alginate/gelatin	Poor printability for cases with acute angles in the scaffold design compared to obtuse and right angles.	[22]
<b>Printing process-related factors</b>			
<i>Pressure</i>			
	Alginate/gelatin	Pressure is the most significant element affecting printability. Excessive pressure can cause poor printability.	[22]
<i>Speed</i>			
	Highly concentrated silver nanoparticle ink	Considering a constant flow rate, lower nozzle speed leads to poor printability due to the extrusion of more bioink per unit time. A high-speed printing nozzle can also lead to discontinuous filaments.	[100]
<i>Cross-linker</i>			
	Alginate-gelatin	A relatively long crosslinking time causes poor printability.	[45]
<i>Nozzle</i>			
	Poly(ethylene glycol)-diacrylate-alginate-	The smaller the nozzle diameter, the higher the resolution and printability.	[101]
	Alginate, photo-crosslinkable polyethylene-glycol diacrylate, gelatin	Not all nozzles with smaller diameters lead to improvements in printability. Nozzles with smaller diameters sometimes require higher pressures to extrude bioinks with lower printability costs.	[102]
	Polyelectrolyte inks	Printability directly corresponds to nozzle size.	[103,104]
<i>Offset (distance between needle and substrate)</i>			
	Alginate	The shorter the distance between the nozzle and a crosslinking agent, the higher the printability.	[105]

[22,89]. These studies are often followed by considering the effect of printing parameters and conditions, as well as the scaffold design, on printability. For example, Kim et al. [90] reported improvements in alginate scaffold printability by adding carrageenan. They first assessed the shear modulus of alginate-based hydrogels to determine the appropriate crosslinking agent. Different concentrations of this hydrogel were then prepared to compare rheological properties and printing resolution. Fig. 15 [24] shows the brief procedure of a regular printability study of four groups of bioinks (3% alginate, 2% alginate + 1% gelatin, 1.5% alginate + 1% gelatin + 0.5% methylcellulose, and 1.5% alginate + 1.5% methylcellulose). In this example, the viscosity of the different groups is evaluated first (Fig. 15A) [24]. A pressure test is then conducted to determine the appropriate pressure at different temperatures and the distances defined between the needle and droplet of bioink, as shown in Fig. 15B [24]. Then, the offset, which is the distance between the needle and printing substrate, is measured (Fig. 15C) [24] to find an appropriate range (offset can affect strand diameter). Finally, a design-related factor such as the angular pattern can be

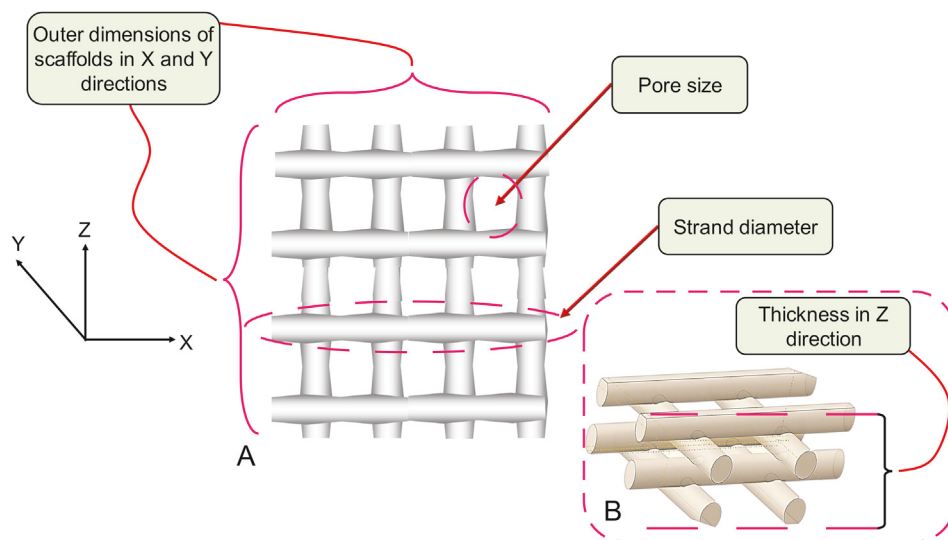
studied to determine its effect on printability (Fig. 15D) [24]. These interrelated factors, as depicted by the printability triangle (Fig. 2 [24]), must be considered in a printability study. As such, the most important task is to identify and limit the number of significantly influential factors; otherwise, reaching a conclusion can be very challenging.

Table 1 provides a general overview of the design, bioink, and fabrication process factors and their influence on the printability of extrusion-based bioprinted scaffolds [22,45,91–105].

#### 4. Printability measurement and characterization

This section reviews and discusses the methods and indexes used to measure and characterize printability for extrusion-based bioprinting. Notably, various methods/indexes have been reported for this purpose; they may not be entirely consistent but are complementary when used to measure printability in terms of the outer geometry and inner structure of scaffolds.

Irregularity is an index used to characterize differences in



**Fig. 16.** Printability study: irregularity measurement in terms of external scaffold dimensions (pore size and strand printability) in (A) X and Y directions, and (B) thickness in Z direction.

overall scaffold dimensions between the scaffold designed and the scaffold printed. Irregularity can be measured in the X, Y, or Z directions as given by the Eq. (9):

$$Irregularity = \frac{|Experimental\ length_{X,Y,Z}|}{Design\ length_{X,Y,Z}} \times 100 \tag{9}$$

where the experimental length is the dimension of the scaffold after printing, and design length is the design dimensions in the X, Y, or Z direction (Fig. 16). The irregularity of a scaffold specifies the overall accuracy of the printed scaffold in comparison to its design in terms of outer geometry, but not internal structure. Compared to irregularity in the X and Y directions, irregularity in the Z direction or in terms of thickness of a scaffold has been more widely used as an essential index of printability [24].

Pore printability is an index that characterizes the difference in pore size/shape between the scaffold designed and scaffold printed (Eq. (10)) and can be defined as [85]:

$$Pore\ printability = \frac{(perimeter\ of\ pore)^2}{16 \times area\ of\ pore} \tag{10}$$

where the perimeter and area of each pore can be calculated by considering each pore in a scaffold structure. As the irregularity index is based on outer geometry, this pore printability index is complementary as it focuses on the internal scaffold geometry [24].

Strand printability is a concept that helps measure printability in terms of comparing the experimental strand diameter to the idealistic (designed) strand diameter. To calculate the idealistic strand diameter, Eq. (11) shows that the relationship between needle speed,  $v$ ; flow rate of a bioink,  $Q$ ; and ideal strand diameter,  $D_s$ ; can be used [106]:

$$D_s = \sqrt{\frac{4Q}{\pi v}} \tag{11}$$

Hence, at different speeds, the ideal strand diameter can be calculated and compared with the experimental strand diameter, and an index for strand printability is then defined as follows (Eq. (12)):

$$Strand\ printability = \frac{Experimental\ strand\ diameter}{D_s} \times 100 \tag{12}$$

where experimental strand diameter is the average strand diameter of a printed scaffold.

For example, the pore printability of a modified alginate scaffold was reported to be between 0.95 and 1.1 (for nozzle speeds of 6–12 mm/s) using Eq. (10); for the same nozzle speeds, strand printability was calculated as 0.7 to 1.0, using Eq. (12) [107].

Strand deflection is another imperfection observed in the structure of scaffolds, as shown in Fig. 6. Deflection is affected by scaffold design, that is, the distance between the strands of scaffolds defined in the designed model can affect deflection. The deflection of strands printed with various pore sizes is measured to evaluate the deflection value and structural integrity. In this test, the side views of the strands are observed, and the deflection ratio can be measured as follows (Eq. (13)):

$$Deflection\ ratio = \frac{Experimental\ area}{Theoretical\ area} \times 100 \tag{13}$$

where the experimental and theoretical areas are the measured and ideal areas after printing, respectively. This deflection ratio can be studied and the scaffold design is modified accordingly. For instance, a shorter distance between strands can be selected to lower the deflection. Increasing the viscosity also decreases the deflection rate. For low-viscosity bioinks, the deflection ratio increases as the distance increases [29]. The results of a deflection test can be used to select an appropriate pore size to reduce the deflection ratio.

The last parameter to evaluate strand printability is surface roughness. The surface roughness of the scaffolds is characterized by studying fluctuations in the surface. At high pressures during bioplotting, bioinks behave like a shear-thinning material and have a smooth surface owing to the considerable surface tension [43]. The surface roughness of scaffolds fabricated from different compositions of bioinks is a subject in need of further study.

Another term, called fidelity, can be defined to measure printability as follows (Eq. (14)):

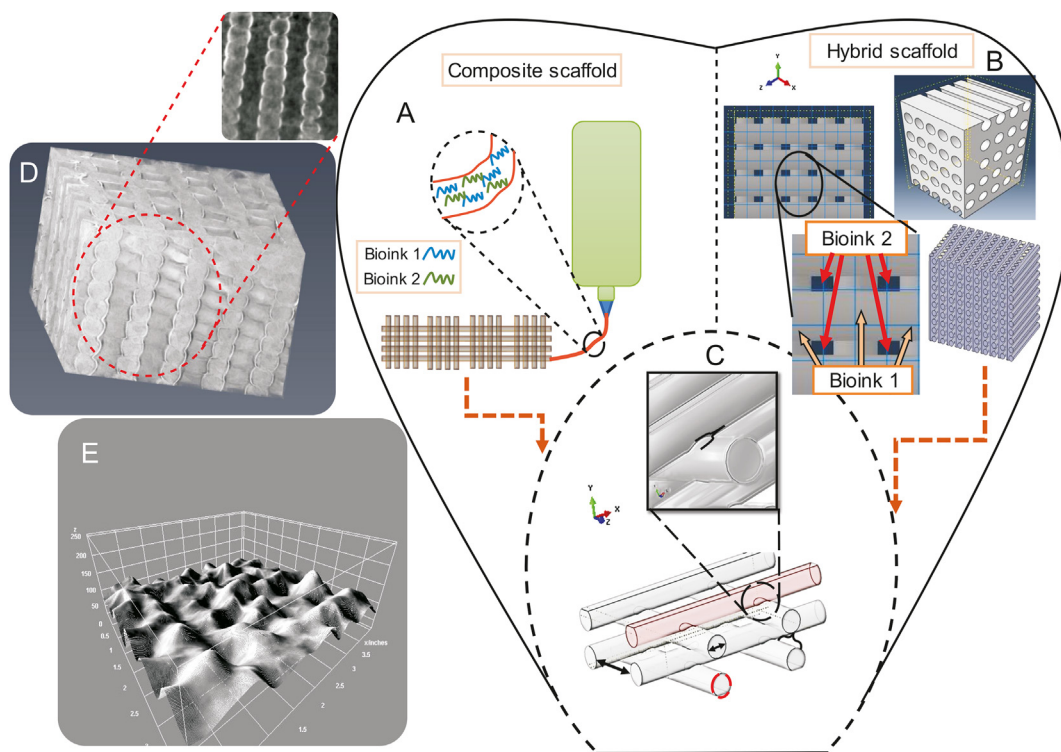


**Fig. 17.** Schematics of models used to represent the configuration of (A) composite scaffolds and (B) hybrid scaffolds; (C) parameters defined in the models (pore size, strand diameter, and penetration amongst layers); (D) novel imaging techniques used for modelling purposes (inset shows a cross-sectional view of a bioprinted alginate scaffold using synchrotron imaging); and (E) topology of a scaffold surface.

$$\text{Fidelity} = \frac{H_p}{H_d} \times 100\% \quad (14)$$

where  $H_p$  is the filament height after printing and  $H_d$  is the filament height in the scaffold design. Using this index, printability can be estimated in terms of how close the printed result is to the actual scaffold design.

As shown in Fig. 6, a filament collapse test can measure the deflection of scaffold strands. Using this concept, hangability can be defined as follows (Eq. (15)):

$$\text{Hangability} = \frac{\text{Actual area}}{\text{Theoretical area}} \times 100\% \quad (15)$$

where the theoretical area is the area below the strand considering the initial scaffold design, and the actual area is the area below the deflected strand after printing. Hangability can also be defined as the distance between the lowest section of a strand and the substrate. No deflection would mean that the distance between the strand and substrate is the actual scaffold design distance; the presence of deflection would reduce this distance.

Extrudability is another index used to evaluate printability [108] and is the minimum pressure required to extrude a material (Fig. 15B) [24]. Another term called the uniformity factor is the diameter of a printed strand divided by the strand's diameter in the designed model. In addition, an integrity factor can be defined by comparing the thickness of the printed scaffold and the developed model. Overall, various indexes can be defined to compare scaffold designs with experimental results in terms of geometrical features to evaluate printability. However, considering one of these factors in isolation is not an appropriate method to assess printability. For example, a printed scaffold with good pore printability might not

have good strand printability. Therefore, multiple indexes are recommended for a more consistent evaluation of printability from different aspects.

## 5. Methods for improving printability

Various studies have aimed to improve printability, resulting in methods to select and regulate printing process-related parameters rigorously, refine and optimize scaffold designs, and develop new bioinks with appropriate properties as well as novel techniques for bioprinting. Scaffold design-related factors that can affect printability are discussed in Section 3.1. With knowledge of these factors, scaffold designs can be modified in terms of pore size, angular pattern, and layer thickness selection to improve printability.

Another area of interest that has recently attracted attention is empirical models that quantify the influence of the printing process-, bioink-, and scaffold design-related parameters on printability [23,69,109]. These models can be implemented to predict the mechanical behavior of scaffolds, a critical aspect of scaffold development. The numerical models currently available can predict the mechanical behavior of scaffolds, such as the elastic modulus [73,75]. Future models should be developed to predict the mechanical characteristics of hybrid and composite scaffolds (Fig. 17). As noted above, an aspect of printability studies is improving printability in terms of developing new bioinks, and new models will be required to predict the mechanical behavior of new composite and hybrid scaffolds. In terms of modeling, new techniques such as synchrotron imaging [110,111] can be used to improve the models developed by adding the real profile of scaffolds as an input (Figs. 17D and E). A recent modeling approach simulates printing resolution for various printing parameters [90].

From a printing process point of view, printability can be studied

from different angles. First, printing parameters such as speed and pressure can be investigated to identify the most significant factors affecting printability. From another perspective, new techniques can be developed to improve printability. While modulations of bioink- and scaffold design-related elements are known approaches to enhancing the printability of hydrogel scaffolds, current research gaps include using other printing process-related approaches, such as indirect bioprinting, to address the poor printability of low-viscosity bioinks.

Indirect bioprinting involves using a sacrificial mold developed through rapid prototyping (RP, another term for AM), casting of the bioink into the mold, and then removing the mold to obtain the final construct [112,113]. This technique is useful for printing low-concentration hydrogels, which are in demand based on evidence supporting the use of a low hydrogel/crosslinker concentration due to positive effects on cell viability. For instance, efforts have been made to use low concentration and soft hydrogels to enable neuron regeneration by providing an adhesive matrix [84,114]. As another example, Matyash et al. [115] reported the utilization of soft alginate hydrogels to support rat and human neuron growth with successful results. While the mechanical properties of low-concentration hydrogels create a favorable cellular environment, they are challenging to print into complex scaffolds [116]. The limited mechanical and physical stability makes such scaffolds prone to collapse and deformation [22,117]. High-resolution 3D printing of low-concentration bioinks is an area of considerable interest, but has not been fully researched [69]. Indirect bioprinting is being explored to overcome these limitations. This opens up the possibility of combining many materials in one scaffold, including bioactive materials, and eliminating concerns related to cell death caused by printing.

Another technique that can be used to improve printability is coaxial nozzle printing. This technique has been used to create vessel-like constructs [11] and can also improve printability. Using this technique, a bioink can be printed as the core, and a crosslinker can be used as the shell. Hence, the bioink is crosslinked immediately after extrusion, which results in a lower chance of bioink spreading due to gravity and surface tension.

Despite significant progress in new bioink development, the need remains for bioinks with improved printability while still considering cell viability [118]. Nanoscale additives can be included in bioinks to improve their shear thinning behavior and, as a result, their printability; such an approach can also improve their mechanical characteristics [119]. Moreover, the crosslinking mechanism of bioinks should be carefully selected. Simultaneous crosslinking of bioinks during the printing process or after printing is relatively slow and can affect printability [120]. Another requirement to keep in mind is that bioinks often shrink after printing; therefore, achieving the desired scaffold requires the design of constructs with larger dimensions that will ultimately match the desired scaffold design after shrinkage. In addition, printability is defined as the capability to form and maintain reproducible 3D scaffolds from bioinks. Hence, printability is not just limited to scaffolds immediately after printing, but reflects how they retain their structure after printing. To this end, printability studies should be conducted on scaffolds in which degradation and swelling ratios are plotted against printability to investigate any printability decrease over time.

## 6. Conclusions

Printability is an important performance index in extrusion-based bioprinting. Herein, we reviewed and described the printing process-, bioink-, and scaffold design-related parameters that affect printability in extrusion-based bioprinting. Many parameters

or factors are involved in the bioprinting process, which affect printability. Notably, the concept of printability has been inconsistently defined and used in the literature, and as such, different indexes and methods have been developed to measure and characterize printability. This review describes our definition of printability and identifies the printability indexes associated with the scaffold printing process, design, and bioink. We believe that printability can be characterized in terms of extrudability and fiber fidelity, as well as factors related to scaffold design. Layer thickness, pore size, and strand orientation are important factors of scaffold design, which affect printability. In addition, methods to enhance printability are discussed, so are the seldom-addressed roles of surface tension and contact angle in modulating printability. The effects of critical printing process parameters and conditions such as pressure, speed, and crosslinking mechanism on printability are discussed. Recent advances in printing processes, including the indirect printing technique aimed at improving the printability of low-viscosity bioinks, are highlighted and discussed, along with suggestions for future research to improve the printability of extrusion-based bioprinting.

## Declaration of competing interest

The authors declare that there are no conflicts of interest.

## Acknowledgments

The authors acknowledge financial support from the Natural Sciences and Engineering Research Council of Canada (NSERC, Grant No.: RGPIN-2014-05648).

## Appendix A. Supplementary data

Supplementary data to this article can be found online at <https://doi.org/10.1016/j.jpha.2021.02.001>.

## References

- [1] H.W. Kang, S.J. Lee, I.K. Ko, et al., A 3D bioprinting system to produce human-scale tissue constructs with structural integrity, *Nat. Biotechnol.* 34 (2016) 312–319.
- [2] B. Starly, W. Lau, T. Bradbury, et al., Internal architecture design and freeform fabrication of tissue replacement structures, *Comput.-Aided Des.* 38 (2006) 115–124.
- [3] G. Gao, B.S. Kim, J. Jang, et al., Recent strategies in extrusion-based three-dimensional cell printing toward organ biofabrication, *ACS Biomater. Sci. Eng.* 5 (2019) 1150–1169.
- [4] R. Langer, Perspectives and challenges in tissue engineering and regenerative medicine, *Adv. Mater.* 21 (2009) 3235–3236.
- [5] H. Sekine, T. Shimizu, J. Yang, et al., Pulsatile myocardial tubes fabricated with cell sheet engineering, *Circulation* 114 (2006) 187–193.
- [6] A. Atala, S.B. Bauer, S. Soker, et al., Tissue-engineered autologous bladders for patients needing cystoplasty, *Lancet* 367 (2006) 1241–1246.
- [7] G. Matsumura, N. Hibino, Y. Ikada, et al., Successful application of tissue engineered vascular autografts: clinical experience, *Biomaterials* 24 (2003) 2303–2308.
- [8] N. Boucard, C. Vito, D. Agay, et al., The use of physical hydrogels of chitosan for skin regeneration following third-degree burns, *Biomaterials* 28 (2007) 3478–3488.
- [9] P. Macchiarini, P. Jungebluth, T. Go, et al., Clinical transplantation of a tissue-engineered airway, *Lancet* 372 (2008) 2023–2030.
- [10] S. Cebotari, A. Lichtenberg, I. Tudorache, A. Batrinac, et al., Clinical application of tissue engineered human heart valves using autologous progenitor cells, *Circulation* 114 (2006) 1132–1137.
- [11] S. Naghieh, M. Sarker, M. Izadifar, et al., Dispensing-based bioprinting of mechanically-functional hybrid scaffolds with vessel-like channels for tissue engineering applications – a brief review, *J. Mech. Behav. Biomed. Mater.* 78 (2018) 298–314.
- [12] S. Naghieh, Extrusion Bioprinting of Hydrogel Scaffolds: Printability and Mechanical Behaviour, Dissertation, University of Saskatchewan, 2020, <https://harvest.usask.ca/handle/10388/13291?show=full>.
- [13] E. Boccardi, I. V. Belova, G.E. Murch, et al., Oxygen diffusion in marine-derived tissue engineering scaffolds, *J. Mater. Sci. Mater. Med.* 26 (2015) 1–9.

- [14] W.E. Teo, W. He, S. Ramakrishna, Electrospun scaffold tailored for tissue specific extracellular matrix, *Biotechnol. J.* 1 (2006) 918–929.
- [15] A. Gleadall, D. Visscher, J. Yang, et al., Review of additive manufactured tissue engineering scaffolds: relationship between geometry and performance, *Burn, Trauma* 6 (2018), 19.
- [16] J.W. Lee, G. Ahn, J.Y. Kim, et al., Evaluating cell proliferation based on internal pore size and 3D scaffold architecture fabricated using solid freeform fabrication technology, *J. Mater. Sci. Mater.: Med.* 21 (2010) 3195–3205.
- [17] J.M. Sobral, S.G. Caridade, R.A. Sousa, et al., Three-dimensional plotted scaffolds with controlled pore size gradients: effect of scaffold geometry on mechanical performance and cell seeding efficiency, *Acta Biomater.* 7 (2011) 1009–1018.
- [18] M. Domingos, F. Intranuovo, T. Russo, et al., The first systematic analysis of 3D rapid prototyped poly ( $\epsilon$ -caprolactone) scaffolds manufactured through BioCell printing: the effect of pore size and geometry on compressive mechanical behaviour and in vitro hMSC viability, *Biofabrication* 5 (2013), 045004.
- [19] A. Schwab, R. Levato, M. D'Este, et al., Printability and shape fidelity of bioinks in 3D bioprinting, *Chem. Rev.* 120 (2020) 11028–11055.
- [20] G. Gillispie, P. Prim, J. Copus, et al., Assessment methodologies for extrusion-based bioink printability, *Biofabrication* 12 (2020), 022003.
- [21] H. Zhang, Y. Cong, A.R. Osi, et al., Direct 3D printed biomimetic scaffolds based on hydrogel microparticles for cell spheroid growth, *Adv. Funct. Mater.* 30 (2020), 1910573.
- [22] Y. He, F. Yang, H. Zhao, et al., Research on the printability of hydrogels in 3D bioprinting, *Sci. Rep.* 6 (2016), 29977.
- [23] J. Göhl, K. Markstedt, A. Mark, et al., Simulations of 3D bioprinting: predicting bioprintability of nanofibrillar inks, *Biofabrication* 10 (2018), 034105.
- [24] S. Naghieh, M.D. Sarker, N.K. Sharma, et al., Printability of 3D printed hydrogel scaffolds: influence of hydrogel composition and printing parameters, *Appl. Sci.* 10 (2020), 292.
- [25] L. Ruiz-Cantu, A. Gleadall, C. Faris, et al., Characterisation of the surface structure of 3D printed scaffolds for cell infiltration and surgical suturing, *Biofabrication* 8 (2016), 015016.
- [26] D.W. Huttmacher, T. Schantz, I. Zein, et al., Mechanical properties and cell cultural response of polycaprolactone scaffolds designed and fabricated via fused deposition modeling, *J. Biomed. Mater. Res.* 55 (2001) 203–216.
- [27] A.D. Olubamiji, Z. Izadifar, J.L. Si, et al., Modulating mechanical behaviour of 3D-printed cartilage-mimetic PCL scaffolds: influence of molecular weight and pore geometry, *Biofabrication* 8 (2016), 025020.
- [28] L. Moroni, J.R. de Wijn, C.A. van Blitterswijk, 3D fiber-deposited scaffolds for tissue engineering: influence of pores geometry and architecture on dynamic mechanical properties, *Biomaterials* 27 (2006) 974–985.
- [29] A. Habib, V. Sathish, S. Mallik, et al., 3D printability of alginate-carboxymethyl cellulose hydrogel, *Materials* 11 (2018), 454.
- [30] M.A. Habib, B. Khoda, Support grain architecture design for additive manufacturing, *J. Manuf. Process.* 29 (2017) 332–342.
- [31] D. Therriault, S.R. White, J.A. Lewis, Rheological behavior of fugitive organic inks for direct-write assembly, *Appl. Rheol.* 17 (2007), 10112.
- [32] A.K.M. Khoda, I.T. Ozbolat, B. Koc, A functionally gradient variational porosity architecture for hollowed scaffolds fabrication, *Biofabrication* 3 (2011), 034106.
- [33] A. Cutolo, B. Neirinck, K. Lietaert, et al., Influence of layer thickness and post-process treatments on the fatigue properties of CoCr scaffolds produced by laser powder bed fusion, *Addit. Manuf.* 23 (2018) 498–504.
- [34] Z. Izadifar, X. Chen, W. Kulyk, Strategic design and fabrication of engineered scaffolds for articular cartilage repair, *J. Funct. Biomater.* 3 (2012) 799–838.
- [35] Q. Zhang, X. Yang, P. Li, et al., Bioinspired engineering of honeycomb structure—Using nature to inspire human innovation, *Prog. Mater. Sci.* 74 (2015) 332–400.
- [36] C. Kucukgul, B. Ozler, H.E. Karakas, et al., 3D hybrid bioprinting of macrovascular structures, *Procedia Eng.* 59 (2013) 183–192.
- [37] J.E. Snyder, Q. Hamid, C. Wang, et al., Bioprinting cell-laden matrigel for radioprotection study of liver by pro-drug conversion in a dual-tissue microfluidic chip, *Biofabrication* 3 (2011), 034112.
- [38] C. Fleming, S. Walker, C. Branyan, et al., Toolpath Planning for Continuous Extrusion Additive Manufacturing, Technical Report, Oregon State University, 2017, <http://people.tamu.edu/~ergun/hyperseeing/2017/06/FASE/5.pdf>.
- [39] J. Warner, P. Soman, W. Zhu, et al., Design and 3D printing of hydrogel scaffolds with fractal geometries, *ACS Biomater. Sci. Eng.* 2 (2016) 1763–1770.
- [40] B. Zhang, P. Jaiswal, R. Rai, et al., Additive manufacturing of functionally graded material objects: a review, *J. Comput. Inf. Sci. Eng.* 18 (2018), 41002.
- [41] G.H. Loh, E. Pei, D. Harrison, et al., An overview of functionally graded additive manufacturing, *Addit. Manuf.* 23 (2018) 34–44.
- [42] J.M. Lee, W.Y. Yeong, Design and printing strategies in 3D bioprinting of cell-hydrogels: a review, *Adv. Healthc. Mater.* 5 (2016) 2856–2865.
- [43] H. Ding, R.C. Chang, Printability study of bioprinted tubular structures using liquid hydrogel precursors in a support bath, *Appl. Sci.* 8 (2018), 403.
- [44] J.H.Y. Chung, S. Naficy, Z. Yue, et al., Bio-ink properties and printability for extrusion printing living cells, *Biomater. Sci.* 1 (2013) 763–773.
- [45] L. Ouyang, R. Yao, Y. Zhao, et al., Effect of bioink properties on printability and cell viability for 3D bioplotting of embryonic stem cells, *Biofabrication* 8 (2016), 035020.
- [46] L.E. Bertassoni, J.C. Cardoso, V. Manoharan, et al., Direct-write bioprinting of cell-laden methacrylated gelatin hydrogels, *Biofabrication* 6 (2014), 024105.
- [47] T. Gao, G.J. Gillispie, J.S. Copus, et al., Optimization of gelatin-alginate composite bioink printability using rheological parameters: a systematic approach, *Biofabrication* 10 (2018), 034106.
- [48] J. Park, S.J. Lee, S. Chung, et al., Cell-laden 3D bioprinting hydrogel matrix depending on different compositions for soft tissue engineering: characterization and evaluation, *Mater. Sci. Eng. C Mater. Biol. Appl.* 71 (2017) 678–684.
- [49] M. Domingos, F. Chiellini, A. Gloria, et al., Effect of process parameters on the morphological and mechanical properties of 3D bioextruded poly ( $\epsilon$ -caprolactone) scaffolds, *Rapid Prototyp. J.* 18 (2012) 56–67.
- [50] R. Frischknecht, C.I. Seidenbecher, The crosstalk of hyaluronan-based extracellular matrix and synapses, *Neuron Glia Biol.* 4 (2008) 249–257.
- [51] C. Rhiner, M.O. Hengartner, Sugar antennae for guidance signals: syndecans and glypicans integrate directional cues for navigating neurons, *Sci. World J.* 6 (2006) 1024–1036.
- [52] T. Andersen, P. Auk-Emblem, M. Dornish, 3D cell culture in alginate hydrogels, *Microarrays (Basel)* 4 (2015) 133–161.
- [53] S.H. Ahn, H.J. Lee, J.-S. Lee, et al., A novel cell-printing method and its application to hepatogenic differentiation of human adipose stem cell-embedded mesh structures, *Sci. Rep.* 5 (2015), 13427.
- [54] R.A. Perez, M. Kim, T.-H. Kim, et al., Utilizing core-shell fibrous collagen-alginate hydrogel cell delivery system for bone tissue engineering, *Tissue Eng. A* 20 (2013) 103–114.
- [55] S.P.M. Bohari, D.W.L. Hukins, L.M. Grover, Effect of calcium alginate concentration on viability and proliferation of encapsulated fibroblasts, *Biomed. Mater. Eng.* 21 (2011) 159–170.
- [56] T. Jiang, J.G. Munguia-Lopez, S. Flores-Torres, et al., Extrusion bioprinting of soft materials: an emerging technique for biological model fabrication, *Appl. Phys. Rev.* 6 (2019) 11310.
- [57] P. Heidarian, A. Kouzani, A. Kaynak, et al., Dynamic hydrogels and polymers as inks for 3D printing, *ACS Biomater. Sci. Eng.* 5 (2019) 2688–2707.
- [58] F. You, X. Wu, X. Chen, 3D printing of porous alginate/gelatin hydrogel scaffolds and their mechanical property characterization, *Int. J. Polym. Mater. Polym. Biomater.* 66 (2016) 299–306.
- [59] A. Ito, A. Mase, Y. Takizawa, et al., Transglutaminase-mediated gelatin matrices incorporating cell adhesion factors as a biomaterial for tissue engineering, *J. Biosci. Bioeng.* 95 (2003) 196–199.
- [60] T. Pan, W. Song, X. Cao, et al., 3D bioplotting of gelatin/alginate scaffolds for tissue engineering: influence of crosslinking degree and pore architecture on physicochemical properties, *J. Mater. Sci. Technol.* 32 (2016) 889–900.
- [61] M. Govindharaj, U.K. Roopavath, S.N. Rath, Valorization of discarded Marine Eel fish skin for collagen extraction as a 3D printable blue biomaterial for tissue engineering, *J. Clean. Prod.* 230 (2019) 412–419.
- [62] M.Y. Teo, L. Stuart, H. Devaraj, et al., The in situ synthesis of conductive polyaniline patterns using micro-reactive inkjet printing, *J. Mater. Chem. C* 7 (2019) 2219–2224.
- [63] H.K. Cader, G.A. Rance, M.R. Alexander, et al., Water-based 3D inkjet printing of an oral pharmaceutical dosage form, *Int. J. Pharm.* 564 (2019) 359–368.
- [64] Z. Zhang, Y. Li, S. Zhu, et al., Patterning catalyst via inkjet printing to grow single-walled carbon nanotubes, *Chin. Chem. Lett.* 30 (2019) 505–508.
- [65] S. Kyle, Z.M. Jessop, A. Al-Sabah, et al., 'Printability' of candidate biomaterials for extrusion based 3D Printing: state-of-the-art, *Adv. Healthc. Mater.* 6 (2017), 1700264.
- [66] X.B. Chen, H. Ke, Effects of fluid properties on dispensing processes for electronics packaging, *IEEE Trans. Electron. Packag. Manuf.* 29 (2006) 75–82.
- [67] W. Aljohani, M.W. Ullah, W. Li, et al., Three-dimensional printing of alginate-gelatin-agar scaffolds using free-form motor assisted microsyringe extrusion system, *J. Polym. Res.* 25 (2018), 62.
- [68] F. Chen, D. Zhang, Q. Yang, et al., Bioinspired wetting surface via laser microfabrication, *ACS Appl. Mater. Interfaces* 5 (2013) 6777–6792.
- [69] E.N. Udofia, W. Zhou, A guiding framework for microextrusion additive manufacturing, *J. Manuf. Sci. Eng.* 141 (2019), 50801.
- [70] Y. Jin, W. Chai, Y. Huang, Printability study of hydrogel solution extrusion in nanoclay yield-stress bath during printing-then-gelation biofabrication, *Mater. Sci. Eng. C Mater. Biol. Appl.* 80 (2017) 313–325.
- [71] S. Vafaei, C. Tuck, I. Ashcroft, et al., Surface microstructuring to modify wettability for 3D printing of nano-filled inks, *Chem. Eng. Res. Des.* 109 (2016) 414–420.
- [72] S. Naghieh, M.D. Sarker, E. Abelseh, et al., Indirect 3D bioprinting and characterization of alginate scaffolds for potential nerve tissue engineering applications, *J. Mech. Behav. Biomed. Mater.* 93 (2019) 183–193.
- [73] S. Naghieh, M.R. Karamooz-Ravari, M. Sarker, et al., Influence of crosslinking on the mechanical behavior of 3D printed alginate scaffolds: experimental and numerical approaches, *J. Mech. Behav. Biomed. Mater.* 80 (2018) 111–118.
- [74] Database of Pixabay, <https://pixabay.com/>. (Accessed 30 April 2019).
- [75] S. Naghieh, M. Sarker, M. Karamooz-Ravari, et al., Modeling of the mechanical behavior of 3D bioplotting scaffolds considering the penetration in interlocked strands, *Appl. Sci.* 8 (2018), 1422.
- [76] Y. Jin, D. Zhao, Y. Huang, Study of extrudability and standoff distance effect during nanoclay-enabled direct printing, *Bio-Des. Manuf.* 1 (2018) 123–134.
- [77] S. Vafaei, D. Wen, T. Borca-Tasciuc, Nanofluid surface wettability through asymptotic contact angle, *Langmuir* 27 (2011) 2211–2218.
- [78] H. Amani, H. Arzaghi, M. Bayandori, et al., Controlling cell behavior through

- the design of biomaterial surfaces: a focus on surface modification techniques, *Adv. Mater. Interfaces* 6 (2019), 1900572.
- [79] J.E. Trachtenberg, P.M. Mountziaris, J.S. Miller, et al., Open-source three-dimensional printing of biodegradable polymer scaffolds for tissue engineering, *J. Biomed. Mater. Res. A* 102 (2014) 4326–4335.
- [80] R. Tripathi, B. Mishra, Development and evaluation of sodium alginate–polyacrylamide graft–co-polymer-based stomach targeted hydrogels of famotidine, *AAPS PharmSciTech* 13 (2012) 1091–1102.
- [81] C.H. Yang, M.X. Wang, H. Haider, et al., Strengthening alginate/polyacrylamide hydrogels using various multivalent cations, *ACS Appl. Mater. Interfaces* 5 (2013) 10418–10422.
- [82] H. Lee, S. Ahn, L.J. Bonassar, et al., Cell(MC3T3-E1)-Printed Poly( $\epsilon$ -caprolactone)/Alginate hybrid scaffolds for tissue regeneration, *Macromol. Rapid Commun.* 34 (2013) 142–149.
- [83] S. Ahn, H. Lee, L.J. Bonassar, et al., Cells (MC3T3-E1)-laden alginate scaffolds fabricated by a modified solid-freeform fabrication process supplemented with an aerosol spraying, *Biomacromolecules* 13 (2012) 2997–3003.
- [84] A. Banerjee, M. Arha, S. Choudhary, et al., The influence of hydrogel modulus on the proliferation and differentiation of encapsulated neural stem cells, *Biomaterials* 30 (2009) 4695–4699.
- [85] M. Ariful Islam Sarker, M. Izadifar, D. Schreyer, et al., Influence of ionic cross linkers (Ca<sup>2+</sup>/Ba<sup>2+</sup>/Zn<sup>2+</sup>) on the mechanical and biological properties of 3D bioprinted hydrogel scaffolds, *J. Biomater. Sci. Polym. Ed.* 29 (2018) 1126–1154.
- [86] X. Liu, S.D. Carter, M.J. Renes, et al., Development of a coaxial 3D printing platform for biofabrication of implantable islet-containing constructs, *Adv. Healthc. Mater.* 8 (2019), 1801181.
- [87] G. Gao, J.Y. Park, B.S. Kim, et al., Coaxial cell printing of freestanding, perfusable, and functional in vitro vascular models for recapitulation of native vascular endothelium pathophysiology, *Adv. Healthc. Mater.* 7 (2018), 1801102.
- [88] D.J. Whyte, R. Rajkhowa, B. Allardyce, et al., A review on the challenges of 3D printing of organic powders, *Bioprinting* 16 (2019), e00057.
- [89] A.I. Cernescu, A. Lungu, I.-C. Stancu, et al., Bioinspired 3D printable pectin-nanocellulose ink formulations, *Carbohydr. Polym.* 220 (2019) 12–21.
- [90] M.H. Kim, Y.W. Lee, W.-K. Jung, et al., Enhanced rheological behaviors of alginate hydrogels with carrageenan for extrusion-based bioprinting, *J. Mech. Behav. Biomed. Mater.* 98 (2019) 187–194.
- [91] S. V. Murphy, A. Skardal, A. Atala, Evaluation of hydrogels for bio-printing applications, *J. Biomed. Mater. Res. A* 101 (2013) 272–284.
- [92] J. Jia, D.J. Richards, S. Pollard, et al., Engineering alginate as bioink for bioprinting, *Acta Biomater.* 10 (2014) 4323–4331.
- [93] B. Duan, E. Kapetanovic, L.A. Hockaday, et al., Three-dimensional printed trileaflet valve conduits using biological hydrogels and human valve interstitial cells, *Acta Biomater.* 10 (2014) 1836–1846.
- [94] K. Markstedt, A. Mantas, I. Tournier, et al., 3D bioprinting human chondrocytes with nanocellulose–alginate bioink for cartilage tissue engineering applications, *Biomacromolecules* 16 (2015) 1489–1496.
- [95] K.S. Lim, B.S. Schon, N.V. Mekhileri, et al., New visible-light photoinitiating system for improved print fidelity in gelatin-based bioinks, *ACS Biomater. Sci. Eng.* 2 (2016) 1752–1762.
- [96] H. Li, S. Liu, L. Lin, Rheological study on 3D printability of alginate hydrogel and effect of graphene oxide, *Int. J. Bioprint.* 2 (2016) 163–175.
- [97] S. Wüst, M.E. Godla, R. Müller, et al., Tunable hydrogel composite with two-step processing in combination with innovative hardware upgrade for cell-based three-dimensional bioprinting, *Acta Biomater.* 10 (2014) 630–640.
- [98] K. Sun, T. Wei, B.Y. Ahn, et al., 3D printing of interdigitated Li-Ion micro-battery architectures, *Adv. Mater.* 25 (2013) 4539–4543.
- [99] A. Piqué, D.B. Chrisey, Direct-Write Technologies for Rapid Prototyping Applications: Sensors, Electronics, and Integrated Power Sources, Academic Press, Elsevier, 2002.
- [100] B.Y. Ahn, S.B. Walker, S.C. Slimmer, et al., Planar and three-dimensional printing of conductive inks, *J. Vis. Exp.* 58 (2011), e3189.
- [101] L.A. Hockaday, K.H. Kang, N.W. Colangelo, et al., Rapid 3D printing of anatomically accurate and mechanically heterogeneous aortic valve hydrogel scaffolds, *Biofabrication* 4 (2012), 035005.
- [102] K.H. Kang, L.A. Hockaday, J.T. Butcher, Quantitative optimization of solid freeform deposition of aqueous hydrogels, *Biofabrication* 5 (2013), 035001.
- [103] G.M. Gratson, J.A. Lewis, Phase behavior and rheological properties of polyelectrolyte inks for direct-write assembly, *Langmuir* 21 (2005) 457–464.
- [104] B. Li, P.A. Clark, K.H. Church, Robust Direct-Write Dispensing Tool and Solutions for Micro/Meso-Scale Manufacturing and Packaging, in: International Manufacturing Science and Engineering Conference, American Society of Mechanical Engineers, 2007, pp. 715–721.
- [105] A.G. Tabriz, M.A. Hermida, N.R. Leslie, et al., Three-dimensional bioprinting of complex cell laden alginate hydrogel structures, *Biofabrication* 7 (2015), 045012.
- [106] M.G. Li, X.Y. Tian, X.B. Chen, Modeling of flow rate, pore size, and porosity for the dispensing-based tissue scaffolds fabrication, *J. Manuf. Sci. Eng.* 131 (2009), 034501.
- [107] M.D. Sarker, S. Naghieh, A.D. McInnes, et al., Bio-fabrication of peptide-modified alginate scaffolds: printability, mechanical stability and neurite outgrowth assessments, *Bioprinting* 14 (2019), e00045.
- [108] N. Soltan, L. Ning, F. Mohabatpour, et al., Printability and cell viability in bioprinting alginate dialdehyde-gelatin scaffolds, *ACS Biomater. Sci. Eng.* 5 (2019) 2976–2987.
- [109] A. Gleadall, I. Ashcroft, J. Segal, VOLCO: a predictive model for 3D printed microarchitecture, *Addit. Manuf.* 21 (2018) 605–618.
- [110] A.D. Olubamiji, Z. Izadifar, N. Zhu, et al., Using synchrotron radiation inline phase-contrast imaging computed tomography to visualize three-dimensional printed hybrid constructs for cartilage tissue engineering, *J. Synchrotron Radiat.* 23 (2016) 802–812.
- [111] A.D. Olubamiji, Z. Izadifar, N. Zhu, et al., Using SR-inline-PCI-CT to visualize 3D-printed hybrid constructs for cartilage tissue engineering, *J. Synchrotron Radiat.* 23 (2016) 802–812.
- [112] C. de Maria, A. de Acutis, G. Vozzi, Chapter 8 – Indirect Rapid Prototyping for Tissue Engineering, in: *Essentials of 3D Biofabrication Translation*, Academic Press, Elsevier, 2015, pp. 153–164.
- [113] A. Houben, J. van Hoorick, J. van Erps, et al., Indirect rapid prototyping: opening up unprecedented opportunities in scaffold design and applications, *Ann. Biomed. Eng.* 45 (2017) 58–83.
- [114] E.K. Purcell, A. Singh, D.R. Kipke, Alginate composition effects on a neural stem cell–seeded scaffold, *Tissue Eng. C Methods* 15 (2009) 541–550.
- [115] M. Matyash, F. Despang, R. Mandal, et al., Novel soft alginate hydrogel strongly supports neurite growth and protects neurons against oxidative stress, *Tissue Eng. A* 18 (2012) 55–66.
- [116] Y. Luo, A. Lode, A.R. Akkineni, et al., Concentrated gelatin/alginate composites for fabrication of pre-designed scaffolds with a favorable cell response by 3D plotting, *RSC Adv.* 5 (2015) 43480–43488.
- [117] B.P. Chan, K.W. Leong, Scaffolding in tissue engineering: general approaches and tissue-specific considerations, *Eur. Spine J.* 17 (2008) 467–479.
- [118] M. Hospodiuk, M. Dey, D. Sosnoski, et al., The bioink: a comprehensive review on bioprintable materials, *Biotechnol. Adv.* 35 (2017) 217–239.
- [119] C. Xu, G. Dai, Y. Hong, Recent advances in high strength and elastic hydrogels for 3D printing in biomedical applications, *Acta Biomater.* 95 (2019) 50–59.
- [120] E.Y.S. Tan, W.Y. Yeong, Concentric bioprinting of alginate-based tubular constructs using multi-nozzle extrusion-based technique, *Int. J. Bioprint.* 1 (2015) 49–56.